CERES_EBAF_Ed4.0

Data Quality Summary (March 7, 2017)

Investigation: **CERES**
Data Product: **EBAF-TOA**

Data Set: **Terra (Instruments: CERES-FM1 or CERES-FM2)**
Aqua (Instruments: CERES-FM3 or CERES-FM4)

Data Set Version: **Edition4.0** **Release Date: March 7, 2017**

CERES Visualization, Ordering and Subsetting Tool: http://ceres.larc.nasa.gov/order_data.php

This document provides a high-level quality assessment of the CERES Energy Balanced and Filled Top-of-Atmosphere (EBAF-TOA) data product. As such, it represents the minimum information needed by scientists for appropriate and successful use of the data product. For a more thorough description of the methodology used to produce EBAF, please see Loeb et al. (2009) and Loeb et al. (2012). A publication summarizing the changes in EBAF Edition 4.0 is in preparation. It is strongly suggested that authors, researchers, and reviewers of research papers re-check this document (especially Cautions and Helpful Hints) for the latest status before publication of any scientific papers using this data product.

Note to Users:

- **To ensure you are using the latest version of EBAF Ed4.0, please check the version and release date in the netCDF file you have against the version and release date in this Data Quality Summary.**
- **EBAF Ed4.0 now provides MODIS-derived cloud properties (cloud fraction, optical depth, effective pressure and effective temperature) alongside TOA fluxes (Section 2.3).**

NOTE: To navigate the document, use the Adobe Reader bookmarks view option. Select "View" "Navigation Panels" "Bookmarks".

TABLE OF CONTENTS

Section Page

LIST OF FIGURES

Figure Page

LIST OF TABLES

Table Page

1. Introduction

CERES instruments fly on the Terra (descending sun-synchronous orbit with an equator crossing time of 10:30 A.M. local time) and Aqua (ascending sun-synchronous orbit with an equator crossing time of 1:30 P.M. local time) satellites. Each CERES instrument measures filtered radiances in the shortwave (SW; wavelengths between 0.3 and 5 μm), total (TOT; wavelengths between 0.3 and 200 μm), and window (WN; wavelengths between 8 and 12 μm) regions. Unfiltered SW, longwave (LW) and WN radiances are determined following Loeb et al. (2001). CERES instruments provide global coverage daily, and monthly mean regional fluxes are based upon complete daily samples over the entire globe.

Despite recent improvements in satellite instrument calibration and the algorithms used to determine SW and LW outgoing top-of-atmosphere (TOA) radiative fluxes, a sizeable imbalance persists in the average global net radiation at the TOA from CERES satellite observations. With the most recent CERES Edition4 Instrument calibration improvements, the SYN1deg_Edition4 net imbalance is ~4.3 W m^{-2}, much larger than the expected observed ocean heating rate ~0.71 W m^{-2} (Johnson et al. 2016). This imbalance is problematic in applications that use Earth Radiation Budget (ERB) data for climate model evaluation, estimations of the Earth's annual global mean energy budget, and studies that infer meridional heat transports. *The CERES Energy Balanced and Filled (EBAF) dataset uses an objective constrainment algorithm to adjust SW and LW TOA fluxes within their ranges of uncertainty to remove the inconsistency between average global net TOA flux and heat storage in the Earth-atmosphere system.*

A second problem users of standard CERES Level-3 data products have noted is the occurrence of gaps in monthly mean clear-sky TOA flux maps due to the absence in some 1°x1° regions of cloud-free areas occurring at the CERES footprint scale (~20-km at nadir). As a result, clear-sky maps from CERES SSF1deg contain many missing regions. *In EBAF, the problem of gaps in clear- sky TOA flux maps is addressed by inferring clear-sky fluxes from both CERES and Moderate Resolution Imaging Spectrometer (MODIS) measurements to produce a new clear-sky TOA flux climatology that provides TOA fluxes in each 1°x1° region every month.*

EBAF Edition4.0 (Ed4.0) leverages off of the many algorithm improvements that have been made in the Edition4 suite of CERES Level 1-3 data products. These include improved instrument calibration, cloud properties, Angular Distribution Models (ADMs) for radiance-to-flux conversion, and use of 1-hourly instead of 3-hourly geostationary imager data for time interpolation. Edition4 products are based upon consistent meteorological assimilation data (GEOS 5.4.1) throughout, and MODIS radiances and aerosols are based upon Collection5 through March 2017 (C6 will supersede C5 starting in April 2017). TOA fluxes are constrained using same approach as EBAF Ed2.8 but using 10 years of Argo (Roemmich et al., 2009) instead of 5 years. For the first time, EBAF will also provide some basic cloud properties derived from MODIS alongside TOA fluxes.

2. Description

The CERES EBAF Ed4.0 product is derived using standard Level 1-3 CERES data products that are the culmination of several processing steps, as summarized in Table 2-1. Raw digitized instrument data (Level 0) are converted to instantaneous filtered radiances (Level 1) using the latest CERES gains (Thomas et al., 2010). Time-dependent spectral response function values are then used to correct for the imperfect spectral response of the instrument and convert the filtered radiances into unfiltered SW, LW and WN radiances (Loeb et al. 2001; Loeb et al., 2016). Since there is no LW channel on CERES, LW daytime radiances are determined from the difference between the TOT and SW channel radiances. Instantaneous TOA radiative fluxes (Level 2) are estimated from unfiltered radiances using empirical ADMs (Su et al., 2015a) for different scene types identified using retrievals from MODIS measurements (Minnis et al. 2011). Their accuracy has been evaluated in several articles (Loeb et al. 2006; Loeb et al. 2007; Kato and Loeb 2005; Su et al., 2015b).

Monthly mean fluxes (Level 3) are determined by spatially averaging the instantaneous TOA flux values on a 1°×1° grid, temporally interpolating between observed values at 1-h increments for each GMT hour of every month, and then averaging all hour boxes in a month (Doelling et al. 2013). CERES employs the CERES-only (CO; CERES SSF1deg stream) and the CERES-geostationary (CG; CERES SYN1deg stream) temporal interpolation methods. The CO method assumes that the cloud properties at the time of the CERES observation remain constant and only accounts for changes in albedo with solar zenith angle and diurnal land heating, by assuming a shape for unresolved changes in the diurnal cycle. The CG method enhances the CERES data by explicitly accounting for changes in cloud and radiation between CERES observation times using 1-hourly imager data from five geostationary (GEO) satellites that cover 60°S-60°N at any given time. During the CERES record, the CERES team has processed data from a total of 18 geostationary imagers of varying quality. With the newest generation of geostationary imagers (e.g., Himawari-8), the quality of the data has improved markedly. Level-3 processing is performed on a nested grid, which uses 1° equal-angle regions between 45°N and 45°S, maintaining area consistency at higher latitudes. The fluxes from the nested grid are then output to a complete 360x180 1°×1° grid using replication.

As described in more detail in the following sections, the EBAF (Level 3B) leverages off of the CERES Level 1-3 data products to produce a monthly TOA flux dataset that maintains the excellent radiometric stability of the CERES instruments while at the same time incorporating diurnal information from geostationary satellites in such a way as to minimize the impact of any geostationary imager artifacts that can occur over some geostationary domains and time periods. In order to ensure EBAF TOA fluxes satisfy known global mean energy budget constraints (e.g., based upon in-situ data from the Argo network), SW and LW TOA fluxes are adjusted within their range of uncertainty using an objective constrainment method (Loeb et al., 2009). ***Importantly, this is a one-time adjustment applied to the entire record. Therefore, the time-dependence of EBAF TOA fluxes is tied to the CERES instrument radiometric stability.*** Unlike other CERES data products, EBAF provides monthly regional clear-sky TOA fluxes that are free of missing regions by making optimal use of coincident CERES and MODIS measurements.

Table 2-1. CERES processing level descriptions.

Level	Description
0	Raw digitized instrument data for all engineering and science data streams in Consultative Committee for Space Data Systems (CCSDS) packet format.
1	Instantaneous filtered broadband radiances at the CERES footprint resolution, geolocation and viewing geometry, solar geometry, satellite position and velocity, and all raw engineering and instrument status data.
2	Instantaneous geophysical variables at the CERES footprint resolution. Includes some Level 1B parameters and retrieved or computed geophysical variables. (e.g., filtered and unfiltered radiances, viewing geometry, radiative fluxes, imager cloud and aerosol properties)
3	Radiative fluxes and cloud properties spatially averaged onto a uniform grid. Includes either instantaneous averages sorted by GMT hour (e.g., SSF1deg–Hour) or temporally interpolated averages at 1–hourly, daily, monthly or monthly hourly intervals (e.g., SSF1deg–Day, -Month, SYN1deg-Hour, -Day, -MHour, -Month).
3B	Level 3 data products adjusted within their range of uncertainty to satisfy known constraints (e.g., consistency between average global net TOA flux imbalance and ocean heat storage).

2.1. All-Sky TOA Flux

CERES_EBAF_4.0 are based upon two data products differentiated by the interpolation methods used:

SSF1deg: The SW radiative fluxes between CERES observation times are determined from the observed fluxes by using scene-dependent diurnal albedo models, which describe how TOA albedo (and therefore flux) changes with solar zenith angle for each local time, assuming the scene properties remain invariant throughout the day. The sun angle–dependent diurnal albedo models are based upon the CERES ADMs developed for the Tropical Rainfall Measuring Mission (TRMM) satellite (Loeb et al. 2003). The LW fluxes in each hour box between CERES observations are determined by linear interpolation of LW fluxes over ocean, while daytime and nighttime observations over land and desert are interpolated by fitting a half-sine curve to the observations to account for the much stronger diurnal cycle over land and desert (Young et al. 1998).

SYN1deg: SW and LW radiative fluxes between CERES observation times are determined by supplementing the CERES observations with 1-hourly TOA fluxes derived from five geostationary satellites covering 60°S-60°N. The geostationary radiances are calibrated against coincident MODIS radiances and TOA flux estimates are normalized against CERES TOA fluxes. Doelling et al. (2013) provides a detailed description of the steps used to estimate broadband TOA fluxes from geostationary imager measurements.

SSF1deg provides global coverage daily with excellent calibration stability, but samples only at specific times of the day due to the sun-synchronous orbit. While the SYN1deg approach provides improved diurnal coverage by merging CERES and 1-hourly geostationary data, artifacts in the GEO data over certain regions and time periods can introduce larger uncertainties. With 1-hourly geostationary sampling, GEO SW fluxes were found to be spurious for solar zenith angles greater than 60° due to the imperfect GEO cloud properties required for the scene

type selection in the narrowband-to-broadband and ADM models used to convert the GEO radiances into SW fluxes. Therefore, sun angle-dependent albedo diurnal models are used to estimate the hourly SW fluxes for solar zenith angles greater than 60° in order to compute the daily flux. In order to remove most of the GEO-derived flux biases, the fluxes are normalized at Terra or Aqua observation times to remain consistent with the CERES instrument calibration (Doelling et al. 2013). Nevertheless, spurious jumps in the SW TOA flux record can still occur when GEO satellites are replaced, due to changes in satellite position, calibration, visible sensor spectral response, cloud retrieval quality, and imaging schedules. Such artifacts in the GEO data can be problematic in studies of TOA radiation interannual variability and/or trends.

To maintain the excellent CERES instrument calibration stability of SSF1deg and also preserve the diurnal information found in SYN1deg, EBAF Ed4.0 uses a new approach involving diurnal correction ratios (DCRs) to convert daily regional mean SSF1deg SW fluxes to diurnally complete values analogous to SYN1deg, but without geostationary artifacts. The DCRs consist of SYN1deg-to-SSF1deg flux ratios sorted by calendar month, surface type, latitude, and a Diurnal Asymmetry Ratio (DAR), defined as follows:

$$DAR = \frac{F^{SW}(morn) - F^{SW}(aft)}{F^{SW}(24h)}$$

where F^{SW}(morn) is the mean SW flux corresponding to 0 h to 12 h local time, F^{SW}(aft) is the mean SW flux corresponding to 12 h to 24 h local time, and F^{SW}(24h) is the mean 24-h SW flux. DAR is derived using geostationary imager radiances only and provides a measure of SW TOA flux difference associated with cloud changes between morning and afternoon. Figure 2-1 provides an example of the regional monthly mean DAR for September 2008. In the stratocumulus regions off the west coasts of North and South America and Africa, DAR is strongly positive since cloud fraction in these regions reaches a maximum in early morning and decreases in the afternoon due mainly to the diurnal cycle of solar insolation and absorption of solar radiation in the upper regions of the cloud (Wood, 2012). Over land, DAR tends to be negative because convection is generally stronger in the afternoon.

For each calendar month, DCRs are defined for ocean, land and desert surfaces (for snow and sea-ice, no correction is applied), at 1° latitude increments centered over ±7.5° latitude intervals, and over DAR increments of 0.05. We use all months between July 2002 and June 2015 to derive the DCRs and only consider the combined Terra-Aqua SYN1deg product to determine the numerator in the SYN1deg-to-SSF1deg ratio as this is the most diurnally complete version available. The denominator is determined either from SSF1deg-Terra or SSF1deg-Terra_Aqua. DCRs generated using only SSF1deg-Terra in the denominator are applied during the Terra-only period (March 2000-June 2002), while a combined Terra-Aqua DCR is used for July 2002-onwards. In the event that Terra or Aqua data are missing during the latter period, DCR corrections based upon Aqua-Only or Terra-Only are used.

Figure 2-2 shows an example of DCRs for ocean centered at 29.5°S in July for Terra-only and for Terra and Aqua combined. Because Terra is a morning satellite, the Terra-based DCR is smaller (greater) than 1 when DAR is positive (negative). The correction reaches 20% at DAR values of

±0.6. In contrast, DCRs when Terra and Aqua are combined are much closer to 1. Thus, the SSF1deg SW flux requires a much smaller diurnal correction when both Terra and Aqua are combined compared to the Terra-only case.

The approach used in Ed4.0 differs from that in Ed2.8, which derived separate scene dependent diurnal corrections for each of the five geostationary satellite domains for each calendar month. EBAF Ed2.8 used MODIS Terra cloud fraction and height retrievals in the scene identification and considered separate ocean, desert, land, marine stratocumulus and land convection categories. The approach used in Ed4.0 in which DCRs are sorted by DAR provides a more direct classification system based upon the strength of the diurnal cycle as opposed to cloud properties.

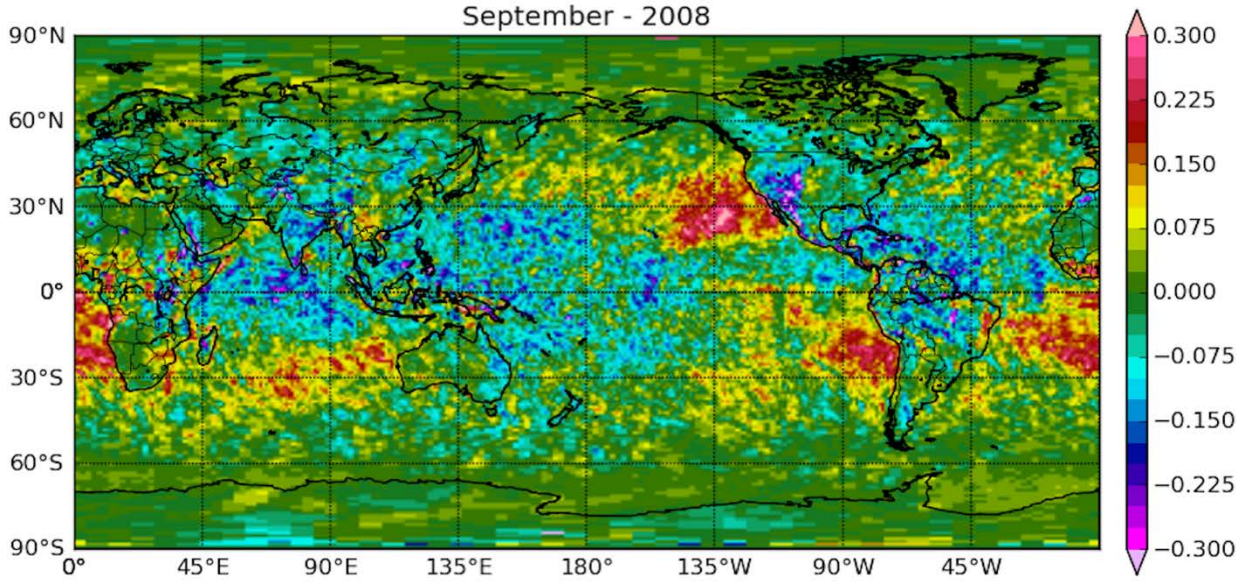

Figure 2-1. Monthly regional mean DAR for September 2008.

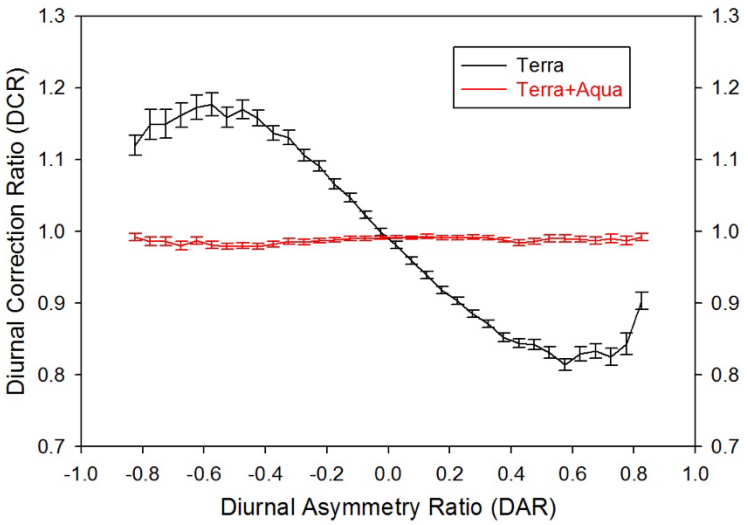

Figure 2-2. DCRs for latitude centered over 29.5°S over ocean in July.

All-sky LW TOA fluxes in EBAF Ed4.0 are derived from SYN1deg determined for Terra only from March 2000-June 2002, and combined Terra and Aqua SYN1deg for July 2002 onwards. In SYN1deg, LW radiative fluxes between CERES observation times are determined by supplementing the CERES observations with data from 5 geostationary satellites that sample every hour for all longitudes between 60°S and 60°N, thus providing the most temporally and spatially complete CERES dataset available. A new geostationary IR imager radiance to LW flux technique was introduced for SYN1deg Ed4. The SYN1deg Ed4 LW fluxes incorporate both the window (11μm) and water vapor (6.7μm) GEO imager channels to determine the LW broadband flux. The geostationary-derived fluxes are normalized to the CERES LW fluxes in order to maintain the CERES instrument calibration. Doelling et al. (2016) provides a detailed description of how broadband TOA fluxes are derived from geostationary data and combined with CERES observations.

Despite recent improvements in satellite instrument calibration and the algorithms used to determine CERES TOA radiative fluxes, a sizeable imbalance persists in the average global net radiation at the TOA from CERES satellite observations. As in previous versions of EBAF (Loeb et al. 2009), the CERES SW and LW fluxes in EBAF Ed4.0 are adjusted within their ranges of uncertainty to remove the inconsistency between average global net TOA flux and heat storage in the Earth–atmosphere system, as determined primarily from ocean heat content anomaly (OHCA) data. In the current version, the global annual mean values are adjusted such that the July 2005–June 2015 mean net TOA flux is 0.71±0.10 W m^{-2} (uncertainties at the 95% confidence level account for XBT correction uncertainties and Argo sampling errors for 0-1800 m) (Johnson et al., 2016). The uptake of heat by the Earth for this period is estimated from the sum of: (i) 0.61±0.09 W m^{-2} from the slope of weighted linear least square fit to ARGO OHCA data to a depth of 1800 m analyzed following Lyman and Johnson (2008); (ii) 0.07±0.04 W m^{-2} from ocean heat storage at depths below 2000 m using data from 1981–2010 (Purkey and Johnson 2010), and (iii) 0.03±0.01 W m^{-2} from ice warming and melt, and atmospheric and lithospheric warming (Rhein et al., 2013). As noted earlier, ***we make a one-time adjustment to the entire record. Therefore, the time-dependence of EBAF TOA fluxes is tied to the CERES instrument radiometric stability.***

2.2. Clear-Sky TOA Flux

Gridbox mean clear-sky TOA fluxes are determined from an area-weighted average of: (i) CERES broadband fluxes from completely cloud-free CERES footprints (20-km equivalent diameter at nadir), and (ii) MODIS-derived "broadband" clear-sky fluxes estimated from the cloud-free portions of CERES footprints with cloud fraction < 95%. In both cases, clear regions are identified using the CERES cloud algorithm applied to MODIS 1-km pixel data (Minnis et al. 2011). Clear-sky fluxes in partly cloudy CERES footprints are derived using MODIS-CERES narrow-to-broadband regressions to convert MODIS narrowband radiances averaged over the clear portions of a footprint to broadband radiances. The narrow-to-broadband regressions are developed from cloud-free CERES footprints from every second year between 2002 and 2014 for Aqua and between 2000 and 2005 for Terra. Separate regressions are derived for each calendar month by combining all Januaries, Februaries, etc., of all years over these periods. Table 2-2 lists the MODIS spectral channels used in the narrow-to-broadband regressions and shows how the regressions are stratified according to surface type, viewing geometry and

precipitable water (LW only). In order to avoid using CERES footprints that likely contain misclassified clear areas due to undetected cloud contamination, the narrow-to-broadband regressions are only applied if the clear area imager 0.65-μm reflectance standard deviation < 0.037 and the 11-μm radiance standard deviation < 0.124 W m^{-2} sr^{-1} μm^{-1}. These thresholds are derived using the 99th percentiles of footprints with a clear fraction >99.9%. Relative to all non-overcast CERES footprints, only 0.5% of CERES footprints are rejected based upon these criteria. The "broadband" MODIS radiances are then converted to TOA radiative fluxes using CERES clear-sky ADMs.

Clear-sky monthly mean SW and LW TOA fluxes are determined by inferring TOA fluxes at each hour of the month and averaging. SW clear-sky TOA fluxes between observation times are determined from the observed fluxes by using scene-dependent diurnal albedo models to estimate how TOA albedo (and therefore flux) changes with solar zenith angle for each local time, assuming the scene properties remain invariant throughout the day. LW clear-sky TOA fluxes between observation times are determined by linear interpolation of LW fluxes over ocean and by applying a half-sine fit during daytime and nighttime over land and desert. Therefore, for monthly mean clear-sky TOA fluxes, we do not explicitly account for changes in the physical properties of the scene (e.g., aerosols, surface properties) during the course of the day.

In determining monthly mean clear-sky SW TOA fluxes from daily mean values, the daily mean SW fluxes are weighted by the gridbox clear area fraction in order to minimize the influence of cloud contamination on the monthly mean clear-sky SW TOA flux. Cloud contamination can occur due to subpixel scale clouds (e.g., trade cumulus) and/or enhanced scattering from adjacent clouds into the clear regions. Indeed, daily mean clear-sky SW TOA fluxes show a linear increase with gridbox cloud fraction that exceeds theoretical values accounting for increases in aerosol humidification near clouds, implying that there likely are some misidentified clear areas on days when cloud amount is appreciable. Weighting the daily mean SW clear-sky fluxes by the gridbox clear area fraction reduces the influence of days with possible cloud contamination on the monthly mean. In contrast, daily mean clear-sky LW TOA fluxes are weighted equally when computing gridbox monthly mean values. Clear-sky LW TOA fluxes show little correlation to cloud fraction. Offline Fu-Liou radiative transfer model calculations of LW TOA flux initialized using temperature and humidity profiles from GOES5 reproduce the spread in daily mean values during the course of a month. We suspect that for SW, subpixel low clouds are the main reason for the correlation between clear-sky flux and cloud fraction. In the LW, low cloud contamination is less critical than cloud contamination by high clouds, which are more extensive and thus more likely to be resolved at the MODIS pixel scale. Furthermore, weighting of LW by clear fraction would mask the effects of upper tropospheric humidity (UTH) variability on clear-sky LW.

In both SW and LW, a correction to narrow-to-broadband bias errors is made monthly based upon the difference between broadband radiances for cloud-free CERES footprints and the MODIS-based broadband estimate. This ensures that the final product's calibration is tied to CERES.

Clear-sky TOA fluxes are derived from Terra prior to July 2002 and Aqua thereafter. MODIS-Aqua is preferred over MODIS-Terra after July 2002 because it is more stable radiometrically

throughout the Aqua period, especially for the water vapor channel. In order to avoid a clear-sky TOA flux discontinuity between the Terra-only (March 2000-June 2002) and Aqua periods (July 2002 onwards), an adjustment is applied to clear-sky fluxes during the Terra-only period. The adjustment is derived using data from 2003-2007. For each calendar month, we compute the regional climatology of the Aqua-Terra difference, and use that difference to adjust Terra clear-sky fluxes during the Terra-only period. The adjustment removes first-order Terra-Aqua differences, thereby avoiding a discontinuity due to inconsistencies between Terra and Aqua clear-sky algorithms (cloud mask, ADMs, etc.).

It should be noted that while EBAF clear-sky TOA fluxes are representative of cloud-free areas, most climate models compute clear-sky fluxes in both clear and cloudy regions assuming there are no clouds present in the gridbox. Because relative humidity in cloud columns is generally greater than in adjacent clear areas, this can lead to a "wet bias" in the models and cause a lower clear-sky LW TOA flux compared to observations. As an example, Figure 2-3 compares clear-sky LW TOA flux calculations obtained from clear and cloudy columns assuming no clouds are present (i.e., by "removing" clouds from cloudy columns) with fluxes weighted by the clear area fraction, analogous to what is done in observations. Differences tend to be larger in regions with persistent high cloud such as over the South Pacific and South Atlantic Convergence Zones and over the West Tropical Pacific. Here the bias reaches -6 W m^{-2}, but Sohn et al. (2006) note that it can reach 10 W m^{-2}. At the global scale, the mean difference is -1.25 W m^{-2}. For clear-sky SW, the global mean difference is only 0.24 W m^{-2}.

Table 2-2. Specific information about the narrow-to-broadband regressions used to infer broadband radiances from MODIS narrowband channels.

Shortwave Narrowband-to-Broadband Regressions	
MODIS Spectral Channels (μm)	0.47, 0.65, 0.86, and 1.63 (Terra) or 2.3 (Aqua)
Surface Types	Ocean, Forests, Savannas, Grassland/Crops, Dark Desert, Bright Desert, Fresh Snow, Sea-Ice, Permanent Snow (Greenland, Antarctica)
Viewing Zenith Angle	7 bins from 0°-70° in 10° increments
Solar Zenith Angle	9 bins from 0°-90° in 10° increments
Relative Azimuth Angle	9 bins from 0°-180° in 20° increments
Longwave Narrowband-to-Broadband Regressions (Separate for Daytime & Nighttime)	
MODIS Spectral Channels (μm)	6.7, 8.5, 11.0, 12.1 and 14.2
Surface Types	Same as for SW (above)
VZA	Same as for SW (above)
Precipitable Water (cm)	0.0-1.0, 1.0-3.0, 3.0-5.0 & 5.0-10.0 (snow/sea-ice free) 0.0-0.2, 0.2-0.4, 0.4-0.6 & 0.6-10 (snow/sea-ice)

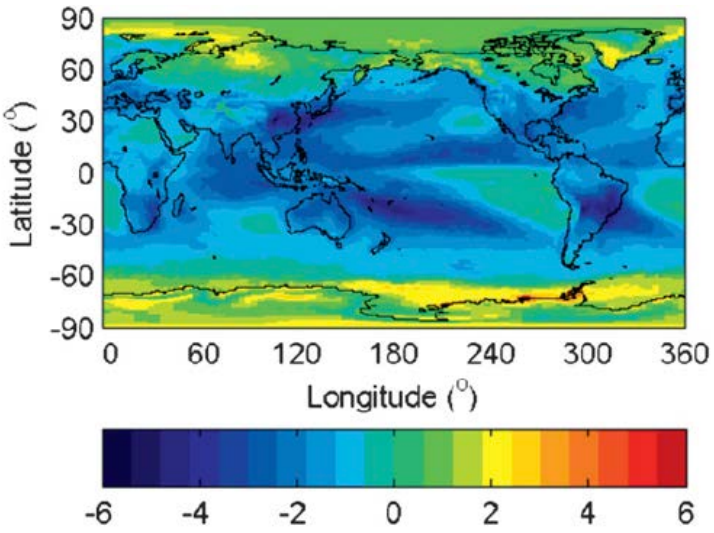

Figure 2-3. Difference between computed clear-sky LW TOA flux (W m^{-2}) obtained by ignoring clouds in cloudy columns (i.e., by "removing" clouds from cloudy columns) and by clear-area weighting regional mean clear-sky fluxes. The calculations are based upon 10 years of monthly gridded mean fluxes from March 2000 through February 2010. (from Kato et al., 2013).

2.3. Cloud Properties

EBAF-TOA Ed4.0 provides MODIS-based monthly mean cloud properties alongside TOA fluxes. The cloud properties include cloud amount, optical depth, effective pressure and temperature derived from instantaneous cloud retrievals averaged over CERES footprints provided in the CERES SSF Ed4 product. The instantaneous cloud properties in SSF Ed4 are based upon an updated methodology to that described in Minnis et al. (20111). For a description of the methodology and accuracy of instantaneous cloud properties in CERES SSF Ed4, please refer to the SSF Ed4.0 Data Quality Summary:

https://eosweb.larc.nasa.gov/project/ceres/quality_summaries/CER_SSF_Terra-Aqua_Edition4A.pdf

In EBAF Ed4.0, the cloud optical depths are based upon daytime MODIS retrievals only, while the remaining cloud properties are computed using both daytime and nighttime data. The monthly mean cloud properties between March 2000 and June 2002 are retrieved from Terra-MODIS, while cloud properties from July 2002 onwards are determined from the average of Terra-MODIS and Aqua-MODIS. Because the Terra-MODIS cloud properties represent the cloud conditions observed during the Terra sun-synchronous orbit overpass time of 10:30 a.m. local equator crossing time, they may differ substantially over maritime stratus and land afternoon convection compared to those during the Terra-Aqua period. As a result, some of the cloud properties may exhibit a discontinuity in some regions in July 2002.

To determine monthly mean cloud properties, we follow the same steps as in the CERES SSF1deg data product. The instantaneous cloud properties in the SSF product are spatially averaged into 1° regions. These are then linearly interpolated hourly to estimate cloud conditions

between the MODIS-observed measurements. The hourly regional cloud properties, whether observed or interpolated, are then averaged over the month. While cloud fraction is simply averaged, the remaining cloud properties are weighted by cloud fraction. Cloud optical depth is averaged in log form, since log cloud optical depth is approximately proportional to visible radiance. The monthly regional cloud properties within a 1° latitude zone are averaged to compute the zonal mean. The global mean cloud properties are averaged from the zonal means using geodetic weighting.

Because the Aqua MODIS 1.6 μm channel failed shortly after launch, the 1.24 μm channel is used as an alternative in both Aqua and Terra Ed4 daytime cloud optical depth retrievals over snow. However, the 1.24 μm channel is not optimal for cloud optical depth since surface reflectance can affect retrievals more than the 1.6 μm channel. Surface shortwave downward flux validation of radiative transfer results over Dome C using 1.6 μm and 1.24 μm cloud retrievals anecdotally suggest that the 1.24 μm cloud optical depths over snow are too large by several percent.

Users interested in a more extensive set of cloud properties at hourly, daily, monthly and monthly hourly timescales are encouraged to consider the SSF1deg or SYN1deg data products, available on the CERES Visualization, Ordering and Subsetting tool:
(**https://ceres.larc.nasa.gov/order_data.php**).

2.4. EBAF Ed4.0 Improvements Over EBAF Ed2.8

While the methodology and input data sets used to produce EBAF Ed4.0 are similar to EBAF Ed2.8, a number of important differences are worth highlighting. EBAF Ed2.8 was based upon essentially a hybrid of versions of CERES algorithms and ancillary input datasets. TOA fluxes were based upon Edition 3 calibration coefficients but the MODIS cloud property retrievals and ADMs used in generating the CERES SSF product were based upon Ed2 algorithms, developed early in the CERES project. The meteorological assimilation data used in the cloud algorithm consisted of GEOS4 for 03/2000-12/2007 and GEOS 5.2.1 for 01/2008-onwards, while MODIS radiance calibration was from Collection 4 for 03/2000-04/2006 and Collection 5 for 05/2006-onwards. Although these input changes have a small impact on all-sky TOA fluxes in EBAF Ed2.8, they do cause discontinuities in clear-sky TOA fluxes (through scene identification). Consequently, users of EBAF Ed2.8 are cautioned about a spurious trend in TOA clear-sky TOA LW flux and therefore LW Cloud Radiative Effect (see EBAF Ed2.8 Data Quality Summary).

EBAF Ed4.0 incorporates all of the algorithm improvements that have recently been implemented in creating the Edition4.0 suite of CERES data products. This includes improved instrument calibration, cloud properties, ADMs and time-interpolation and space averaging with hourly geostationary imager measurements. The meteorological assimilation data used is based upon GEOS 5.4.1 throughout the record and MODIS radiances and aerosol input files are from Collection 5 through March 2017. C5 production is expected to stop after March 2017 and be superseded by Collection 6. As noted earlier, the EBAF Ed4.0 global net TOA flux constraint uses 10 years of Argo instead of 5 years.

EBAF Ed4.0 time-averaging is performed using GMT whereas EBAF Ed2.8 used local time. This has implications for regional solar incoming flux (Section 6). In Ed2.8, the call to solar ephemeris

was once per day for GMT=12 for all regions, whereas for Ed 4.0 we update hourly for each region. We also compute the solar incoming twice for a 1° region at the 0.25° and 0.75° latitudes and then average the results rather than computing it once at the 0.5° midpoint as in Ed2.8. This properly distributes the solar incoming over the polar regions when the sun is rising or setting rapidly.

Substantial algorithm improvements were made in EBAF Ed4.0 clear-sky flux determination. The greatest improvement is associated with the Edition 4 MODIS cloud mask. The new cloud mask substantially improves detection of thin cirrus and low cloud, provides a better discrimination between cloud and dust, and substantially improves cloud detection in polar regions. The cloud mask improvements include the use of additional MODIS channels and threshold tests (MODIS 1.38 μm threshold test, T3.7-T11 and T11-T12 difference tests, 2.1 to 0.6 μm ratio test, 1.24 to 0.65 μm ratio test, and new VIS threshold tests) derived with the benefit of years of CALIPSO data for guidance. In contrast, the EBAF Ed2.8 cloud mask was developed prior to CALIPSO. As noted earlier, the EBAF Ed4.0 narrow-to-broadband regressions now use many spectral channels (Table 2-2). In EBAF Ed2.8, the narrow-to-broadband regression was based upon 0.65, 0.86 and 1.63 μm for SW and only one channel (11 μm) for LW. As a result, the magnitude of the required corrections for narrow-to-broadband error are much smaller in EBAF Ed4.0. In addition, the ADMs used in EBAF Ed4.0 are improved compared to Ed2.8, particularly over ocean and areas affected by heavy aerosol (smoke, dust, pollution) (Su et al., 2015a). In polar regions, EBAF Ed2.8 only estimates a high-resolution clear-sky flux if the CERES footprint is partly cloudy and has 100% sea-ice, 100% open water or 100% land coverage. This conservative approach inadvertently excludes many footprints with high partial sea-ice coverage and causes clear-sky SW TOA flux to be underestimated over summertime Arctic Ocean. This problem is overcome in EBAF Ed4.0, which estimates high-resolution clear-sky flux if CERES footprint is partly cloudy and partly sea-ice/water or partly snow/land. We apply both sets of regressions to clear-sky radiances and weight by surface type coverage. This increases the clear-sky SW TOA flux over Arctic Ocean compared to Ed2.8. EBAF Ed4.0 also corrects a coding error found in EBAF Ed2.8 clear-sky time-space averaging involving erroneous use of all-sky instead of clear-sky directional models (diurnal models of albedo dependence upon solar zenith angle) for converting instantaneous SW TOA clear-sky fluxes into 24-h averages. This correction increases the magnitude of clear-sky SW TOA flux.

3. Cautions and Helpful Hints

The CERES Science Team notes several CAUTIONS and HELPFUL HINTS regarding the use of CERES_EBAF_Ed4.0:

- The CERES_EBAF_Ed4.0 product can be visualized, subsetted, and ordered from: http://ceres.larc.nasa.gov.

(a) TOA Fluxes:

- Users are cautioned that all-sky SW and LW TOA fluxes are determined from Terra only from March 2000-June 2002 and combined Terra and Aqua for July 2002 onwards. Clear-sky TOA fluxes are derived from Terra prior to July 2002 and Aqua thereafter. An adjustment is applied to clear-sky fluxes during the Terra-only period to remove first-order differences between Terra and Aqua. Consequently, uncertainties are slightly larger prior to July 2002 (Section 4).
- The climatological mean values are calculated relative to a base period of July 2005 – June 2015.
- The solar incoming TOA flux is derived from daily SORCE TIM measurements, which have an average annual flux of ~1361 W m^{-2}, vary with time, and take into account the solar sunspot cycle with an amplitude of ~0.1%.
- Clear-sky TOA fluxes in EBAF Ed4.0 are provided for clear regions within CERES footprints from MODIS pixels identified as clear at 1-km spatial resolution. This definition differs from what is used in the standard CERES data products (SSF1deg and SYN1deg), which only provide clear-sky fluxes in regions that are completely cloud-free at the CERES footprint scale. LW TOA fluxes for clear-sky regions identified at the higher spatial resolution are on average 2.3 W m^{-2} lower compared to the standard CERES data products in regions in which a clear-sky LW TOA flux is available in the standard products. The corresponding regional RMS difference is 5.7 W m^{-2}. The difference increases to 4.4 W m^{-2} when all regions with a clear-sky LW TOA flux is available for both approaches. At high latitudes, clear-sky TOA fluxes in the standard CERES products are missing in most regions as fewer footprints are identified as completely cloud-free at the CERES footprint scale. SW TOA fluxes for clear-sky regions identified at the higher spatial resolution are on average 1.5 W m^{-2} higher compared to the standard CERES data products in regions in which a clear-sky SW TOA flux is available in the standard products. The corresponding regional RMS difference is 4.8 W m^{-2}. When all regions with a clear-sky SW TOA flux is available for both approaches, the global mean values are nearly identical. *Users should be aware that both of these definitions of "clear-sky" used for CERES observations might differ from what is used in climate model output. Many models compute clear-sky radiative fluxes in each column, regardless of whether the column is clear or cloudy. Sohn et al. (2006) note that differences in how clear-sky is defined in model output and observations can lead to regional LW TOA flux differences of up to 10 W m^{-2}.*
- In determining monthly mean clear-sky SW TOA fluxes from daily mean values, the daily mean SW fluxes are weighted by the gridbox clear area fraction in order to minimize the influence of cloud contamination on the monthly mean clear-sky SW TOA flux. In contrast, daily mean clear-sky LW TOA fluxes are weighted equally when computing gridbox monthly mean values. For details please see Section 2.2.

- Since TOA flux represents a flow of radiant energy per unit area and varies with distance from the earth according to the inverse-square law, a reference level is also needed to define satellite-based TOA fluxes. From theoretical radiative transfer calculations using a model that accounts for spherical geometry, the optimal reference level for defining TOA fluxes in radiation budget studies for the earth is estimated to be approximately 20 km. At this reference level, there is no need to explicitly account for horizontal transmission of solar radiation through the atmosphere in the earth radiation budget calculation. In this context, therefore, the 20-km reference level corresponds to the effective radiative "top of atmosphere" for the planet. Since climate models generally use a plane-parallel model approximation to estimate TOA fluxes and the earth radiation budget, they implicitly assume zero horizontal transmission of solar radiation in the radiation budget equation and do not need to specify a flux reference level. By defining satellite-based TOA flux estimates at a 20- km flux reference level, comparisons with plane-parallel climate model calculations are simplified since there is no need to explicitly correct plane-parallel climate model fluxes for horizontal transmission of solar radiation through a finite atmosphere. For a more detailed discussion of reference level, please see Loeb et al. (2002).
- When the solar zenith angle is greater than 90°, twilight flux (Kato and Loeb 2003) is added to the outgoing SW flux in order to take into account the atmospheric refraction of light. The magnitude of this correction varies with latitude and season and is determined independently for all-sky and clear-sky conditions. In general, the regional correction is less than 0.5 W m^{-2}, and the global mean correction is 0.2 W m^{-2}. Due to the contribution of twilight, there are regions near the terminator in which outgoing SW TOA flux can exceed the incoming solar radiation. Users should be aware that in these cases, albedos (derived from the ratio of outgoing SW to incoming solar radiation) exceed unity.
- EBAF uses geodetic weighting to compute global means. The spherical Earth assumption gives the well-known $S_o/4$ expression for mean solar irradiance, where S_o is the instantaneous solar irradiance at the TOA. When a more careful calculation is made by assuming the Earth is an oblate spheroid instead of a sphere, and the annual cycle in the Earth's declination angle and the Earth-sun distance are taken into account, the division factor becomes 4.0034 instead of 4. The following file provides the zonal geodetic weights used to determine global mean quantities.
  (http://ceres.larc.nasa.gov/science_information.php?page=GeodeticWeights).

(b) Cloud Properties:

- EBAF Ed4.0 provides MODIS-based cloud properties (cloud fraction, daytime optical depth, effective pressure and effective temperature) from SSF1deg Ed4.0. For March 2000-June 2002, cloud properties are based upon MODIS Terra only (CERES_SSF1deg-Month_Terra-MODIS_Ed4A), whereas cloud properties for July 2002 onwards are given by the average of MODIS Terra and Aqua. No attempt is made to force consistency between the MODIS Terra and MODIS Aqua cloud properties. ***Therefore, cloud properties may exhibit a discontinuity in July 2002 owing to MODIS Terra and Aqua calibration differences and diurnal cloud property differences between the two periods.***
- Because the Aqua MODIS 1.6 μm channel failed shortly after launch, the 1.24 μm channel is used as an alternative in both Aqua and Terra Ed4 daytime cloud optical depth retrievals over snow. However, the 1.24 μm channel is not optimal for cloud optical depth since surface reflectance can affect retrievals more than the 1.6 μm channel. Surface shortwave

downward flux validation of radiative transfer results over Dome C using 1.6 μm and 1.24 μm cloud retrievals anecdotally suggest that the 1.24 μm cloud optical depths over snow are too large by several percent.

- The Terra-MODIS water vapor (6.76-μm) channel performance has degraded after the Terra spacecraft anomaly event (February 18-28, 2016). Because this channel is mostly used to enhance cloud detection during polar night, cloud properties observed before and after the Terra spacecraft anomaly may be inconsistent over Antarctica and the Arctic Ocean during their months of polar night. The TOA LW flux is not affected.
- The climatological mean values are calculated relative to a base period of July 2005 – June 2015.

4. Accuracy and Validation

4.1. Regional Mean All-Sky SW TOA Flux

The uncertainty in 1°x1° regional SW TOA flux is evaluated separately for 03/2000-06/2002 (Terra-Only period) and for 07/2002-onwards (Terra-Aqua period). To determine uncertainties due to temporal interpolation for the Terra-Only period, we use data from the Terra-Aqua period and compare regional fluxes derived by applying DCRs to SSF1deg_Terra with regional fluxes in SYN1deg_Terra_Aqua, which combines CERES observations on Terra, Aqua and five geostationary instruments covering all longitudes between 60°S and 60°N, thus providing the most temporally and spatially complete CERES dataset for diurnal sampling. Temporal interpolation uncertainties for the Terra-Aqua period are determined by comparing regional fluxes derived by applying DCRs to SSF1deg_Terra_Aqua with SYN1deg_Terra_Aqua. For comparison, we also compare SW TOA fluxes from SSF1deg_Terra and SSF1deg_Terra_Aqua directly with those in SYN1deg_Terra_Aqua, which shows the impact of not applying DCRs. Results for the Terra-Only period are shown in Figure 4-1a-b for October 2008. With no diurnal corrections (Figure 4-1a), temporal interpolation errors reach close to 30 W m^{-2} off the coast of South America over marine stratocumulus and -20 W m^{-2} over the land convection regions of South America and Southern Africa. After applying DCRs to SSF1deg_Terra (Figure 4-1b), the errors are significantly reduced. The overall root-mean-square (RMS) error between 60°S and 60°N is reduced from 4.5 to 2.7 W m^{-2} after applying the DCRs. For the Terra-Aqua period, there is a dramatic improvement in the uncorrected SSF1deg result (Figure 4-2a) compared to the Terra-Only case. The regional RMS error for SSF1deg_Terra_Aqua is 2.2 W m^{-2} and the regional RMS error decreases further to 1.9 W m^{-2} after applying DCRs (Figure 4-2b).

If we assume the overall uncertainty is due to: 1) the EBAF diurnal correction, 2) radiance-to-flux conversion error of 1 W m^{-2} (Su et al., 2015b), and 3) CERES instrument calibration uncertainty of 1 W m^{-2} (1σ), the regional uncertainty of all-sky SW TOA flux for EBAF Ed4.0 for March 2000–June 2002 is estimated as sqrt(3^2+1^2 +1^2) or approximately 3 W m^{-2}, and for July 2002-onwards it is estimated as sqrt(2^2+1^2 +1^2) or approximately 2.5 W m^{-2}.

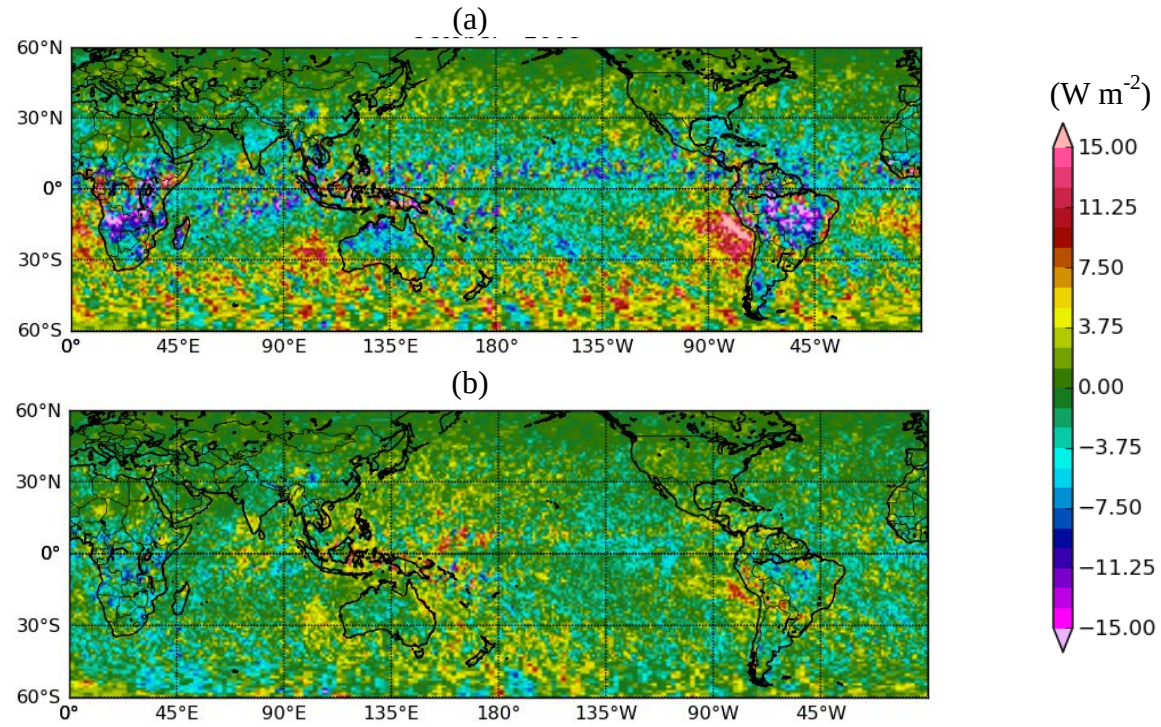

Figure 4-1. All-sky SW TOA flux difference relative to SYN1deg_Terra_Aqua (a) before diurnal correction (SSF1deg_Terra) and (b) after applying DCRs to SSF1deg_Terra for October 2008.

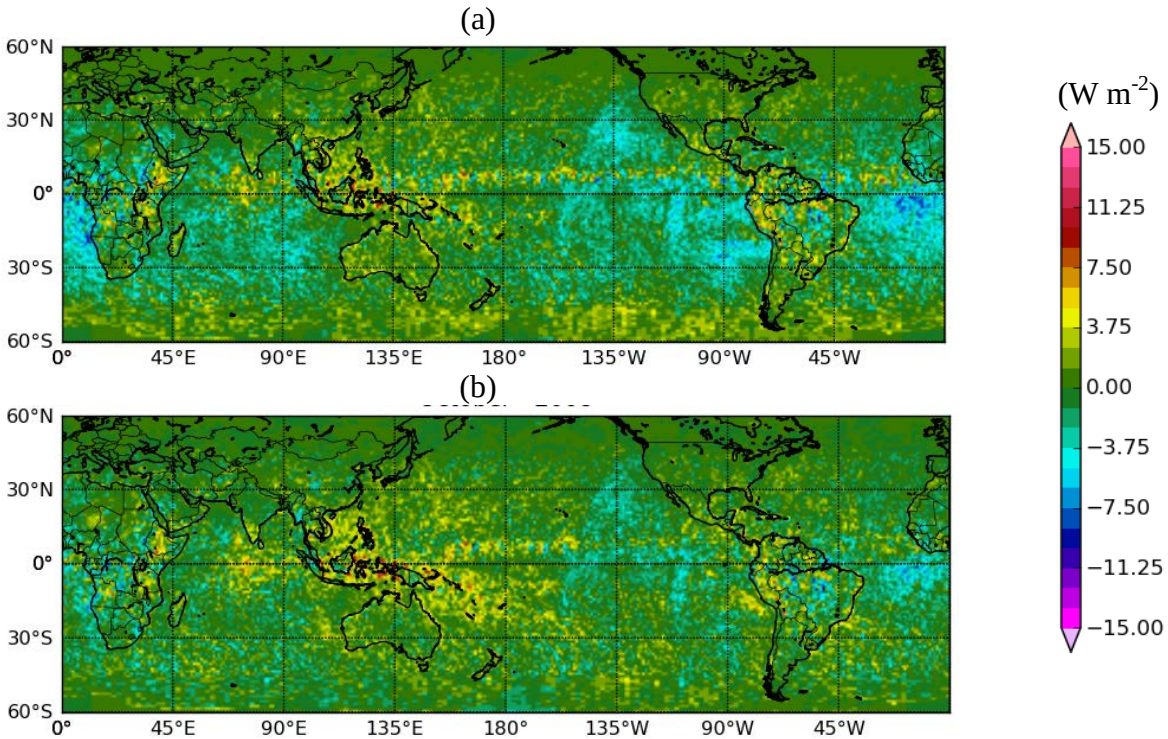

Figure 4-2. All-sky SW TOA flux difference relative to SYN1deg_Terra_Aqua (a) before diurnal correction (SSF1deg_Terra_Aqua) and (b) after applying DCRs for October 2008.

4.2. Regional Mean All-Sky LW TOA Flux

The uncertainty in 1°x1° regional LW TOA flux is evaluated separately for 03/2000-06/2002 (Terra-Only period) and for 07/2002-onwards (Terra-Aqua period). To determine uncertainties due to temporal interpolation for the Terra-Only period, we use data from the Terra-Aqua period and compare regional fluxes between SSF1deg_Terra with regional fluxes in SYN1deg_Terra_Aqua, which combines CERES observations on Terra, Aqua and five geostationary instruments covering all longitudes between 60°S and 60°N, thus providing the most temporally and spatially complete CERES dataset for diurnal sampling. In SSF1deg, linear temporal interpolation between CERES observations is used over ocean whereas a half-sine fit is applied over land to account for daytime heating. Temporal interpolation uncertainties for the Terra-Aqua period are determined by comparing regional fluxes from SSF1deg_Terra_Aqua with SYN1deg_Terra_Aqua. Results for the Terra-Only period are shown in Figure 4-3a for October 2008. LW TOA flux differences are generally less than 5 W m^{-2} except in over Tibet, convective regions in central Africa and mountainous regions in South America. The errors are markedly reduced when both Terra and Aqua are used in SSF1deg (Figure 4-3b). The overall root-mean-square (RMS) error between 60°S and 60°N is 2.2 W m^{-2} for the Terra-only case and 1.4 W m^{-2} when Terra and Aqua are combined.

If we assume the overall uncertainty is due to: 1) the EBAF diurnal correction, 2) radiance-to-flux conversion error of 0.75 W m^{-2} (Su et al., 2015b), and 3) CERES instrument calibration uncertainty of 0.75% or 1.8 W m^{-2} (1σ), the regional uncertainty of all-sky LW TOA flux for EBAF Ed4.0 for March 2000–June 2002 is estimated as sqrt(2.2^2+0.75^2 +1.8^2) or approximately 3 W m^{-2}, and for July 2002-onwards it is estimated as sqrt(1.4^2+0.75^2 +1.8^2) or approximately 2.5 W m^{-2}.

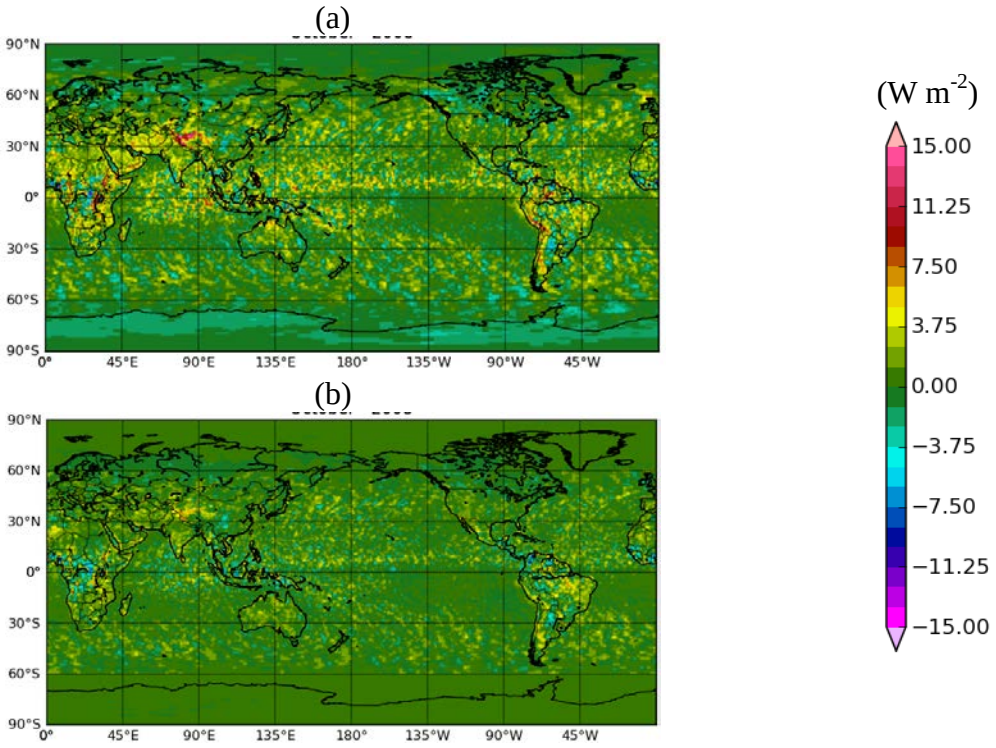

Figure 4-3. All-sky LW TOA flux difference relative to SYN1deg_Terra_Aqua for (a) SSF1deg_Terra and (b) SSF1deg_Terra_Aqua for October 2008.

4.3. Regional Mean Clear-Sky SW TOA Flux

The uncertainty in 1°x1° regional clear-sky SW TOA flux is determined from calibration uncertainty, errors in narrow-to-broadband conversion, radiance-to-flux conversion, time-space averaging, and scene identification. During the Terra-only period, there is also uncertainty due to the adjustment made to Terra clear-sky TOA fluxes, applied to ensure that Terra clear-sky fluxes prior to July 2002 are consistent with those from Aqua after July 2002, thereby minimizing possible discontinuities between the Terra-only and Terra-Aqua periods.

For CERES, calibration uncertainty is 1% (1σ), which for a typical global mean clear-sky SW flux corresponds to ≈0.5 W m^{-2}. The narrow-to-broadband regional RMS error is 0.9 W m^{-2}, determined by applying the narrow-to-broadband regressions to cloud-free CERES footprints and comparing with CERES radiances. For clear-sky SW TOA flux, the radiance-to-flux conversion error contributes 1 W m^{-2} to regional RMS error (Loeb et al. 2007), and time-space averaging adds 2 W m^{-2} uncertainty. The latter is based upon an estimate of the error from TRMM-derived diurnal albedo models that provide albedo dependence upon scene type (Loeb et al. 2003). In EBAF, "clear-sky" is defined as cloud-free at the MODIS pixel scale (1 km). A pixel is identified as clear using spectral MODIS channel information and a cloud mask algorithm (Minnis et al. 2011). Based upon a comparison of SW TOA fluxes for CERES footprints

identified as clear according to MODIS but cloudy according to CALIPSO with TOA fluxes from footprints identified as clear according to both MODIS and CALIPSO, Sun et al. (2011) found that footprints with undetected subvisible clouds reflect 2.5 W m^{-2} more SW radiation compared to completely cloud-free footprints and occur in approximately 50% of footprints identified as clear by MODIS. This implies an error of 1.25 W m^{-2} due to misclassification of clear scenes. For the Terra-Aqua period, the total error in TOA outgoing clear-sky SW radiation in a region is estimated as sqrt(0.5^2+0.9^2+1^2+2^2+1.25^2) or approximately 3 W m^{-2}. For the Terra-only period, the uncertainty due to the adjustment made to Terra clear-sky TOA fluxes is determined by comparing the adjusted Terra clear-sky TOA fluxes with corresponding Aqua values. For March 2003, the regional RMS was 3 W m^{-2} (other months give similar results). Thus for the Terra-only period, the total error in TOA outgoing clear-sky SW radiation in a region is sqrt(0.5^2+0.9^2+1^2+2^2+1.25^2+3.0^2) or approximately 4 W m^{-2}.

4.4. Regional Mean Clear-Sky LW TOA Flux

The uncertainty in 1°x1° regional clear-sky LW TOA flux is determined from calibration uncertainty and errors in narrow-to-broadband conversion, radiance-to-flux conversion, time-space averaging, and scene identification. As for SW, there is also additional uncertainty during the Terra-only period to account for the adjustment made to Terra clear-sky TOA fluxes. For CERES, calibration uncertainty is 0.75% (1σ), which for a typical global mean clear-sky LW flux corresponds to ≈2 W m^{-2}. The narrow-to-broadband regional RMS error is 1.6 W m^{-2}, determined by applying the narrow-to-broadband regressions to cloud-free CERES footprints and comparing with CERES radiances. For clear-sky LW TOA flux, the radiance-to-flux conversion error contributes 0.7 W m^{-2} to regional RMS error (Loeb et al. 2007), and time-space averaging adds 1 W m^{-2} uncertainty. The latter assumes zero error over ocean (i.e., no appreciable diurnal cycle in clear-sky LW) and a 3 W m^{-2} error in the half-sine fit over land and desert (Young et al. 1998). In EBAF, "clear-sky" is defined as cloud-free at the MODIS pixel scale (1 km). A pixel is identified as clear using spectral MODIS channel information and a cloud mask algorithm (Minnis et al. 2011). Based upon a comparison of LW TOA fluxes for CERES footprints identified as clear according to MODIS but cloudy according to CALIPSO with TOA fluxes from footprints identified as clear according to both MODIS and CALIPSO, Sun et al. (2011) found that footprints with undetected subvisible clouds emit 5.5 W m^{-2} less LW radiation compared to completely cloud-free footprints and occur in approximately 50% of footprints identified as clear by MODIS. This implies an error of 2.75 W m^{-2} due to misclassification of clear scenes. The total error in TOA outgoing clear-sky LW radiation in a region is estimated as sqrt(2^2+1.6^2+0.7^2+1^2+2.75^2) or approximately 4 W m^{-2}. For the Terra-only period, the uncertainty due to the adjustment made to Terra clear-sky TOA fluxes is determined by comparing the adjusted Terra clear-sky TOA fluxes with corresponding Aqua values. For March 2003, the regional RMS was 1.8 W m^{-2} (other months give similar results). Thus for the Terra-only period, the total error in TOA outgoing clear-sky LW radiation in a region is sqrt(2^2+1.6^2+0.7^2+1^2+2.75^2+1.8^2) or approximately 4.4 W m^{-2}.

4.5. Solar Incoming Radiation

The CERES science team provides daily and monthly regional mean TOA incident solar flux using various total solar irradiance (TSI) daily datasets (Table 4-1). The TSI values are adjusted to a common reference given by the Solar Radiation and Climate Experiment (SORCE) Total Solar Irradiance (TIM) TSI V-15 dataset. The SORCE TIM instrument measures the absolute intensity of solar radiation, integrated over the entire solar disk and the entire solar spectrum reported at the mean solar distance of 1 astronomical unit (AU). TIM is an ambient temperature active cavity radiometer that uses electrical substitution radiometers (ESRs) to measure TSI to an estimated absolute accuracy of 350 ppm (0.035%). Relative changes in solar irradiance are measured to less than 10 ppm/yr (0.001%/yr), allowing determination of possible long-term variations in the Sun's output (Kopp et al. 2005).

During the early CERES Terra record prior to the launch of SORCE (Mar2000−Feb2003), TSI is provided by data from the WRC file composite_d41_62_0906.dat after applying an offset recommended by the SORCE data providers. From March 2003-July 30, 2013, SORCE TSI V-15 data are used. The SORCE TIM instrument stopped collecting daily TSI after a battery failure on the SORCE satellite on July 30, 2013. Daily TSI data from RMIB-Composite was substituted for SORCE. An offset of 2.4447 W m^{-2} was applied to the RMIB data in consultation with the RMIB team. SORCE data production resumed in March 2014 but CERES continued to use RMIB data until October 2014. In November 2014, CERES resumed the use of SORCE data (now Version 17). A small offset (V15 −V17 = −0.0049 W m^{-2}) was applied to bring V17 in line with V15. V17 data, with the above offset, continues to be used for CERES Ed4A.

A plot of the combined daily TSI is shown in Figure 4-4. The daily TSI that EBAF uses can be obtained at this web site:
http://ceres.larc.nasa.gov/science_information.php?page=TSIdata.

Table 4-1. TSI data sets used in CERES EBAF Ed4.0

Period	TSI Source
March 1, 2000 – February 24, 2003	From Dr. Greg Kopp of LASP, University of Colorado, Boulder, who had extracted it from a composite dataset from the World Radiation Center (WRC), Davos. The file used, "composite_d41_62_0906.dat" was downloaded from the ftp site: ftp://ftp.pmodwrc.ch/pub/data/irradiance/composite. Dr. Kopp had offset WRC-Composite time series to match with the SORCE version available at the time (V-09). We offset the WRC-Composite time series further to match with SORCE V-15 data following the procedure suggested by Dr. Kopp. According to this procedure, the offset between the SORCE time series and another one is determined by comparing the two time series for the period 25Feb2003 to 31Dec2003.
February 25, 2003 – June 30, 2013	SORCE TIM V-15 (Kopp and Lean 2011)

Table 4-1. TSI data sets used in CERES EBAF Ed4.0

Period	**TSI Source**
July 1, 2013 -- October 31, 2014	A composite data set available from the Royal Meteorological Institute of Belgium (RMIB) (Mekaoui and Dewitte 2008). It is based on the DIARAD/VIRGO data set (Dewitte et al. 2004) and absolutely calibrated according to Dewitte et al. 2013. This data set was radiometrically scaled to SORCE TIM V-15 using an offset, which was determined over a 5-year period (01Mar2003 - 29Feb2008).
November 1, 2014 – present	SORCE TIM V-17 with offset of -0.0049 W m^{-2} applied to bring V17 in line with V15.

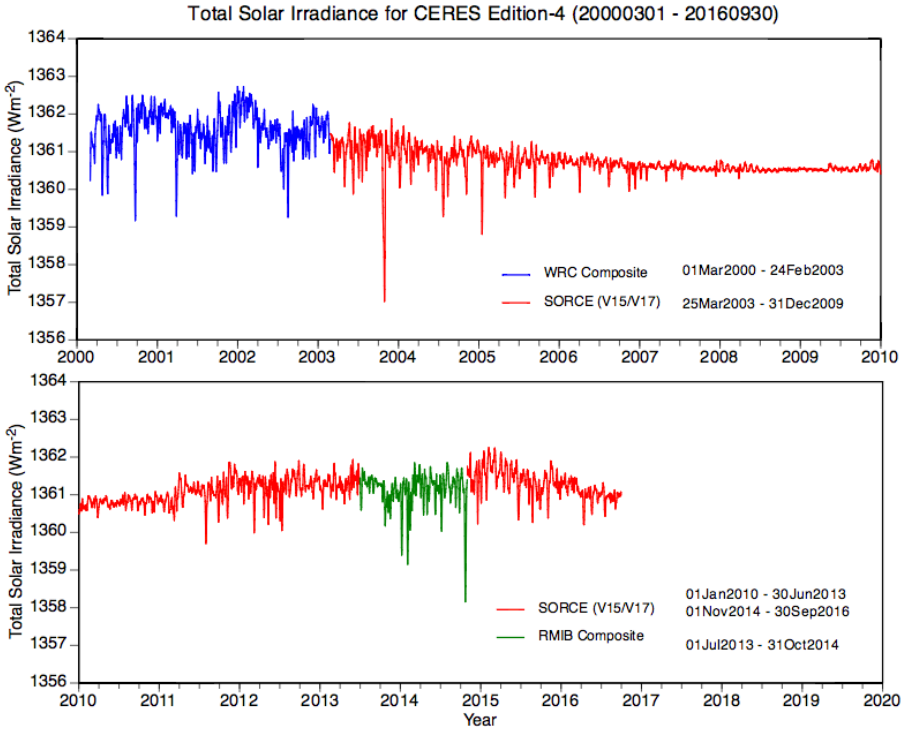

Figure 4-4. TSI composite data from WRC, SORCE(V15) and RMIB for the CERES timeframe.

5. Version History Summary

The CERES project will increment the EBAF version when major changes to either inputs or algorithms are made. However, when minor changes occur, a release will be made without incrementing the version. Instead, we will update the release date in the "Version" global attribute of the netCDF file.

Table 5-1 provides a list of input data products used to create each version of EBAF and also lists the reference providing the global energy imbalance constraint used to anchor the CERES TOA fluxes.

Table 5-1. EBAF input and ocean heating rate constraint.

Version	SW all-sky	LW all-sky	Clear-sky	Global Energy Imbalance Constraint
Ed1	Terra-SYN1deg-lite Ed2.0 (SRBAVG)	Terra-SYN1deg-lite Ed2 (SRBAVG)	Terra-SYN1deg-lite Ed2 (SRBAVG)	Hansen 2005
Ed2.5	Terra-SYN1deg-lite Ed2.5	Terra-SYN1deg-lite Ed2.5	Terra-SSF1deg-lite Ed2.5	Hansen 2005
Ed2.6, Ed2.6r	Terra/Aqua-SSF/SYN1deg-lite Ed2.6	Terra-SYN1deg-lite Ed2.6	Terra-SSF1deg-lite Ed2.6	ARGO-based 2006-2010
Ed2.7	Terra/Aqua-SSF/SYN1deg-lite Ed2.7 (internal)	Terra-SYN1deg-lite Ed2.7 (internal)	Terra-SSF1deg-lite Ed2.7 (internal)	ARGO-based 2006-2010
Ed2.8	Terra/Aqua-SSF/SYN1deg-lite Ed2.7 (internal)	Terra-SYN1deg-lite Ed2.7 (internal)	Terra-SSF1deg-lite Ed2.7 (internal)	ARGO-based 2006-2010
Ed4.0	Terra/Aqua-SSF/SYN1deg-lite Ed4.0 (internal)	Terra/Aqua-SYN1deg-lite Ed4.0 (internal)	Terra-SSF1deg-lite Ed4.0 (03/2000-06-2002) (internal) Aqua-SSF1deg-lite Ed4.0 (07/2002-onwards) (internal)	ARGO-based 07/2005-06/2015

EBAF Edition4.0 was released on February 3, 2017. A second release was made on March 7, 2017, and includes corrections to the following issues in the initial release:

- Part of the EBAF processing failed to account for leap year in 2000. This affected all-sky TOA fluxes during the year 2000.
- The snow-ice SW clear-sky directional models were improperly applied. This affected regional SW clear-sky fluxes over snow-ice regions.
- When there is a data gap in daily SSF1deg all-sky SW flux, the daily SYN1deg SW flux, which contains geostationary SW fluxes, is used as a backup to maintain consistency in daily sampling for monthly SW and LW fluxes. In certain conditions (e.g., oblique viewing zenith

angles and low sun), the SYN1deg SW flux contains unrealistically low SW fluxes due to erroneous geostationary cloud retrievals. In this second release, the problem is overcome by neglecting SYN1deg SW fluxes that are lower than a minimum threshold set by the expected clear-sky ocean SW flux for the corresponding latitude and day of the year. This problem occurs rarely and is mainly found early in the CERES record during the Terra-only period (i.e., prior to July 2002).

- The predominant geostationary satellite may have been incorrectly determined at the boundary between geostationary domains and when an operational satellite was switched during a month. The resulting error in all-sky SW and LW monthly flux was less than 1 W m^{-2}.

6. Difference between EBAF Ed4.0 and EBAF Ed2.8

6.1. Global Mean TOA Flux Comparisons

Table 6-1 compares global TOA averages for EBAF Ed4.0 and Ed2.8. Global mean all-sky TOA fluxes in EBAF Ed4.0 decreases by 0.5 W m^{-2} in the SW and increases by 0.6 W m^{-2} in the LW compared to EBAF Ed2.8. In contrast, much larger differences occur for clear-sky TOA fluxes, with EBAF Ed4.0 increasing by 0.8 W m^{-2} in the SW and 2.7 W m^{-2} in the LW relative to EBAF Ed2.8. As noted earlier, the main reason for the increase in LW clear-sky TOA flux is due to cloud mask changes between Ed4.0 and Ed2.8. The Ed4.0 cloud mask substantially improves detection of thin cirrus and low cloud, provides a better discrimination between cloud and dust, and substantially improves cloud detection in polar regions. Consequently, the EBAF Ed4.0 clear-sky LW TOA flux is much larger than that in EBAF Ed2.8. One might also expect the cloud mask improvements to reduce the EBAF Ed4.0 SW clear-sky TOA flux below that in EBAF Ed2.8. However, improvements in dust detection resulted in more dust in EBAF Ed4.0 SW clear-sky flux, which offset the impact of cloud mask changes elsewhere. In addition, EBAF Ed4.0 corrects a coding error found in EBAF Ed2.8 clear-sky SW TOA flux time-space averaging. In converting gridded average instantaneous clear-sky SW TOA fluxes to 24-h averages, EBAF Ed2.8 inadvertently used all-sky instead of clear-sky diurnal models of the albedo dependence upon solar zenith angle. Correcting this error causes clear-sky SW TOA flux to increase, which further offsets decreases due to cloud mask improvements.

Because of the large changes in clear-sky TOA fluxes, cloud radiative effect (CRE) shows marked differences between EBAF Ed4.0 and Ed2.8. In the LW, CRE increases by 2.2 W m^{-2}, while the magnitude of SW CRE cooling decreases by 1.4 W m^{-2}. Consequently, net CRE changes by 3.4 W m^{-2} between EBAF Ed4.0 and Ed2.8.

Table 6-1. Global mean TOA fluxes (W m^{-2}) from EBAF Ed4.0 and EBAF Ed2.8 for July 2005-June 2015.

	Ed2.8	**Ed4.0**
Incoming Solar	339.8	340.0
All-Sky LW	239.6	240.1
All-Sky SW	99.6	99.1
All-Sky Net	0.63	0.71
Clear-sky LW	265.4	268.1
Clear-Sky SW	52.5	53.3
Clear-Sky Net	21.9	18.6
LW CRE	25.8	28.0
SW CRE	-47.1	-45.8
Net CRE	-21.3	-17.9

6.2. Regional Mean TOA Flux Comparisons

Regional mean TOA flux differences between EBAF Ed4.0 and Ed2.8 for SW all-sky, clear-sky and CRE are shown in Figure 6-1 for March 2000 – June 2015. Figure 6-2 provides the corresponding TOA flux differences for LW. For all-sky SW (Figure 6-1a), EBAF Ed4.0 values exceed Ed2.8 by up to 5 W m^{-2} in stratocumulus regions, corresponding to ≈3% relative to the mean. The difference is due to improvements in the diurnal correction in EBAF Ed4.0 that takes advantage of increased sampling of the diurnal cycle with 1-hourly instead of 3-hourly geostationary imager data in Ed4.0. The overall regional RMS difference between EBAF Ed4.0 and Ed2.8 is 1.3 W m^{-2} (Table 6-2). For clear-sky SW TOA flux, marked differences appear off the coast of Northern Africa due to improvements in EBAF Ed4.0 dust/cloud discrimination. EBAF Ed4.0 values exceed Ed2.8 because Ed4.0 identifies more scenes as dust instead of cloud compared to Ed2.8. Elsewhere over the oceans, EBAF Ed4.0 exceeds Ed2.8 by 2-4 W m^{-2} due mainly to the correction of a coding error found in EBAF Ed2.8 clear-sky SW TOA flux time-space averaging (Section 6.1). Regional differences for SW CRE resemble those for clear-sky SW. The overall regional RMS difference is 3.4 W m^{-2} for clear-sky and 3.6 W m^{-2} for CRE (Table 6-2). In the LW, EBAF Ed4.0 all-sky values are generally within 3 W m^{-2} of EBAF Ed2.8 (Figure 6-2a), and the overall regional RMS difference is 0.8 W m^{-2}. In contrast, the regional pattern of LW clear-sky TOA flux differences (Figure 6-2b) shows much larger differences in regions of persistent high cloud cover, such as over the Indian Ocean, the western tropical Pacific Ocean, the ITCZ, and convective regions over the Amazon and central Africa. In some regions, differences can reach 10 W m^{-2}. The overall regional RMS difference is the same as for SW, 3.4 W m^{-2}. As for SW, the LW CRE pattern resembles that for clear-sky (Figure 6-2c). Regional all-sky net TOA flux differences are generally smaller than 5 W m^{-2} (Figure 6-3a), and the overall regional RMS difference is 1.4 W m^{-2}. For clear-sky (Figure 6-3b), differences over ocean are generally strongly negative since both SW and LW clear-sky TOA flux differences are positive. Over land, net clear-sky TOA flux differences are positive and resemble the pattern of clear-sky SW TOA flux differences. The overall regional RMS is 5.4 W m^{-2}. Net CRE differences (Figure 6-3c) resemble clear-sky but are of opposite sign. The regional RMS difference is 5.3 W m^{-2}.

Regional differences in solar irradiance between EBAF Ed4.0 and Ed2.8 are shown in Figure 6-4 for seasonal months in 2008. The cause of the difference is in the approach used in time-averaging. EBAF Ed4.0 time-averaging is performed using GMT whereas EBAF Ed2.8 used local time. In Ed2.8, the call to solar ephemeris was once per day for GMT=12 for all regions, whereas for Ed 4.0 we update hourly for each region. We also compute the solar incoming twice for a 1° region at the 0.25° and 0.75° latitudes and then average the results rather than computing it once at the 0.5° midpoint as in Ed2.8. This properly distributes the solar incoming over the polar regions when the sun is rising or setting rapidly.

Table 6-2. Regional root-mean-square (RMS) difference between EBAF Ed4.0 and EBAF Ed2.8 for March 2000-June 2015.

	SW	LW	Net
All-Sky	1.3	0.8	1.4
Clear-Sky	3.4	3.4	5.4
CRE	3.6	3.0	5.3

(a)

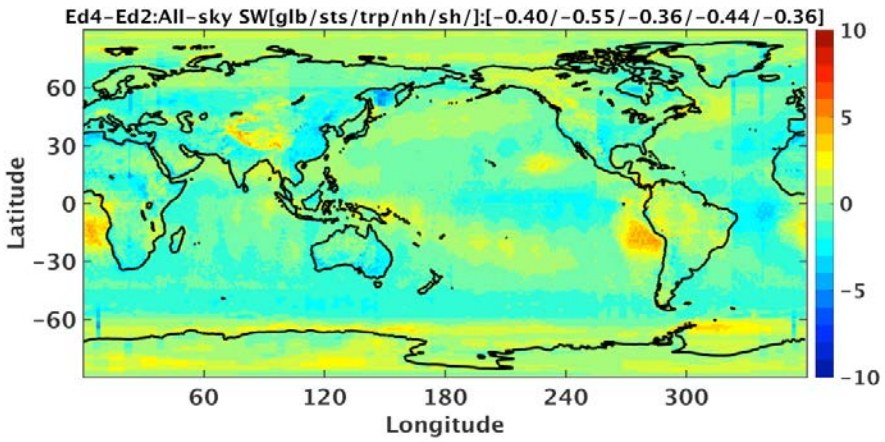

(b)

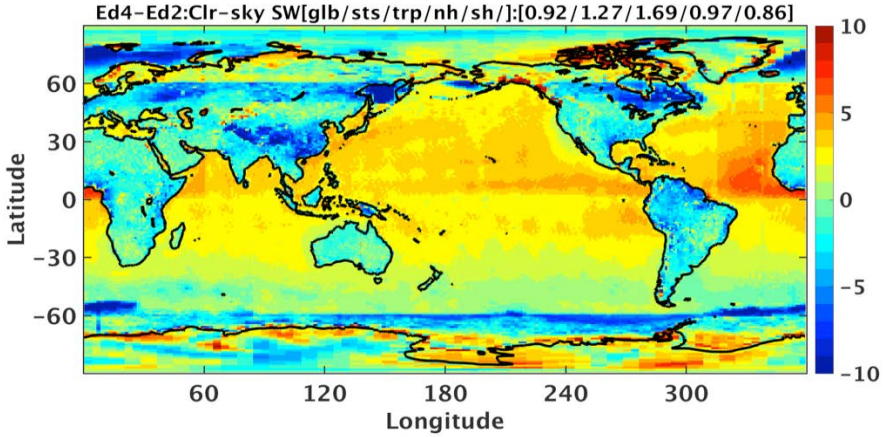

(c)

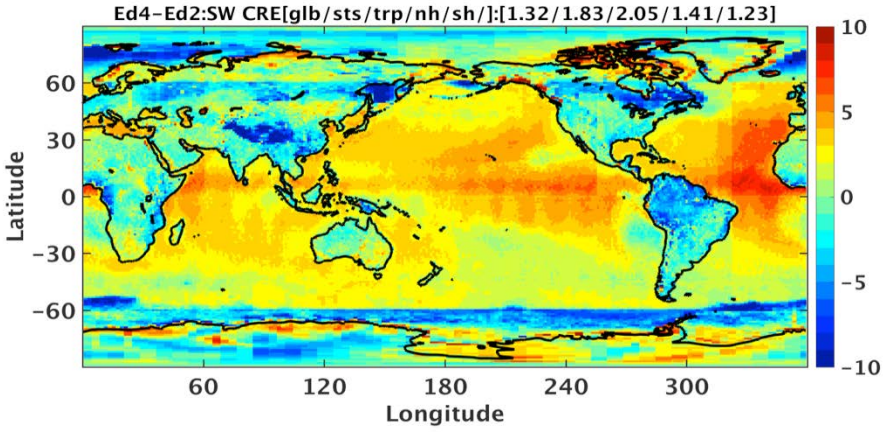

Figure 6-1. EBAF Ed4.0 minus EBAF Ed2.8 SW TOA flux difference for (a) all-sky, (b) clear-sky and (c) CRE for March 2000-June 2015.

(a)

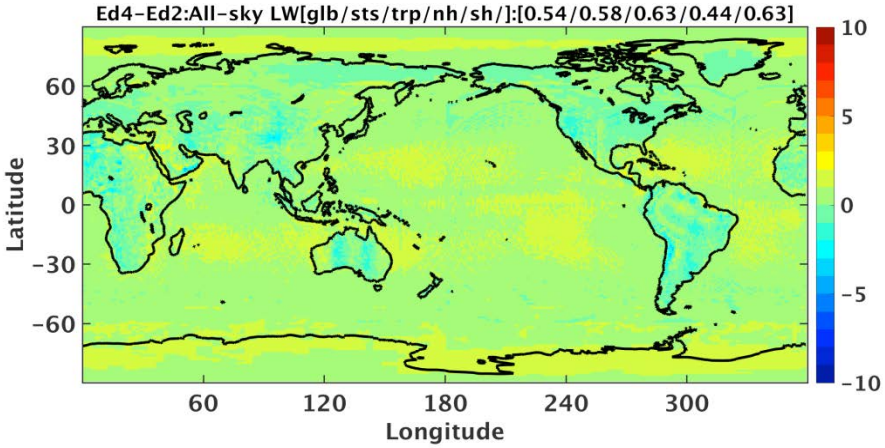

(b)

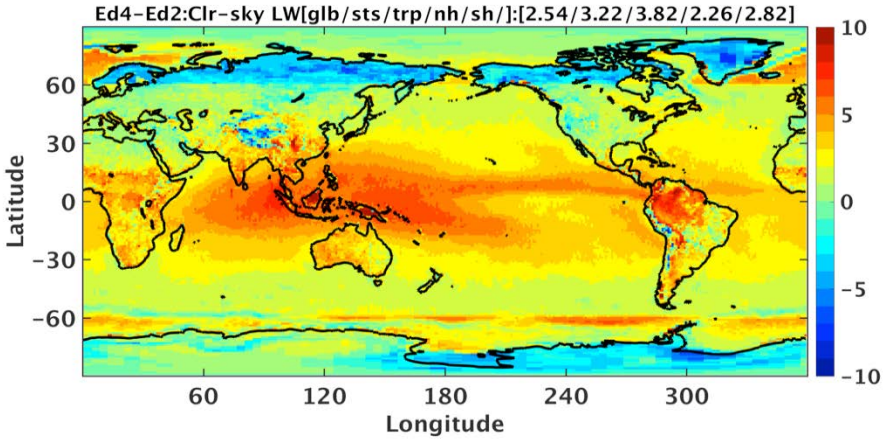

(c)

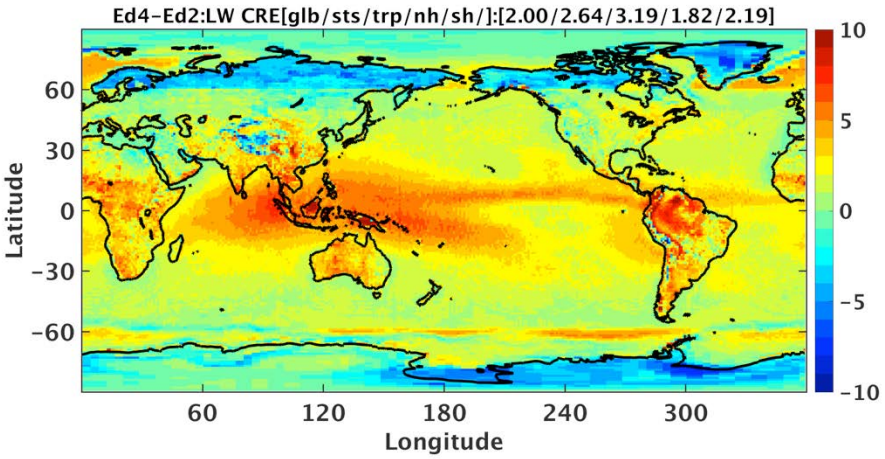

Figure 6-2. Same as Figure 6-1 but for LW.

(a)

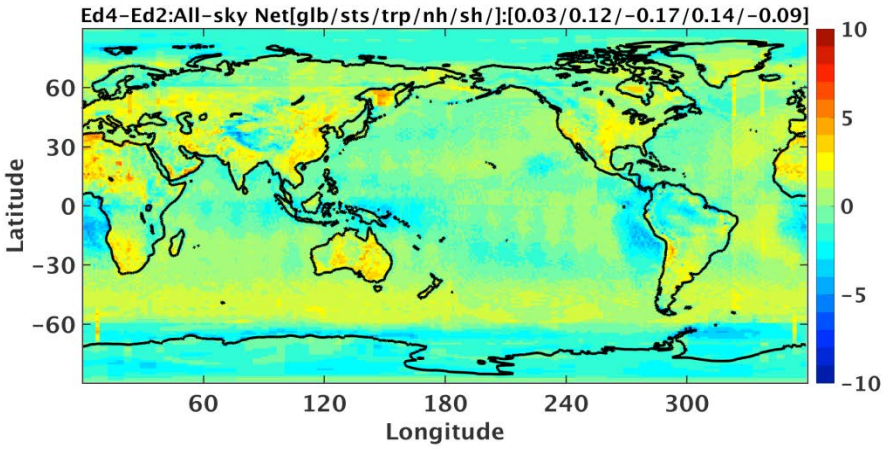

(b)

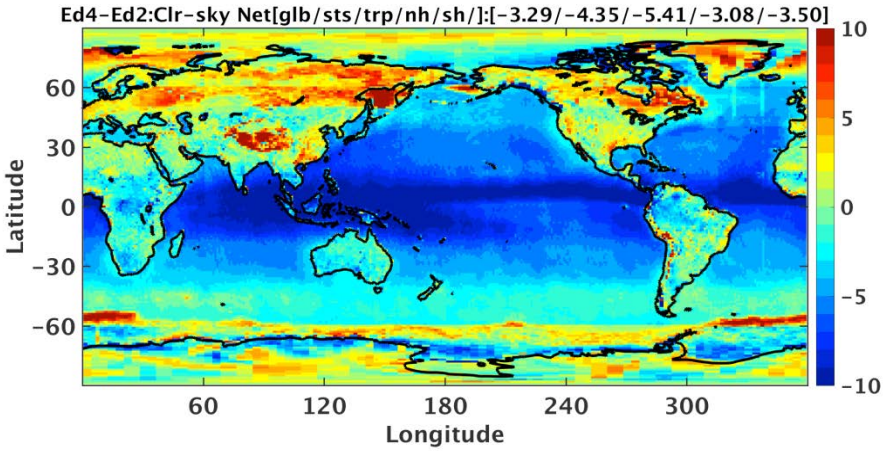

(c)

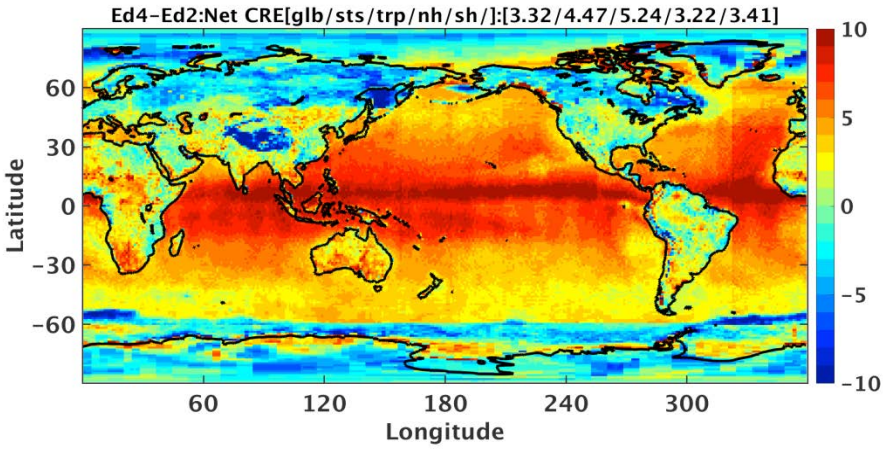

Figure 6-3. Same as Figure 6-1 but for Net.

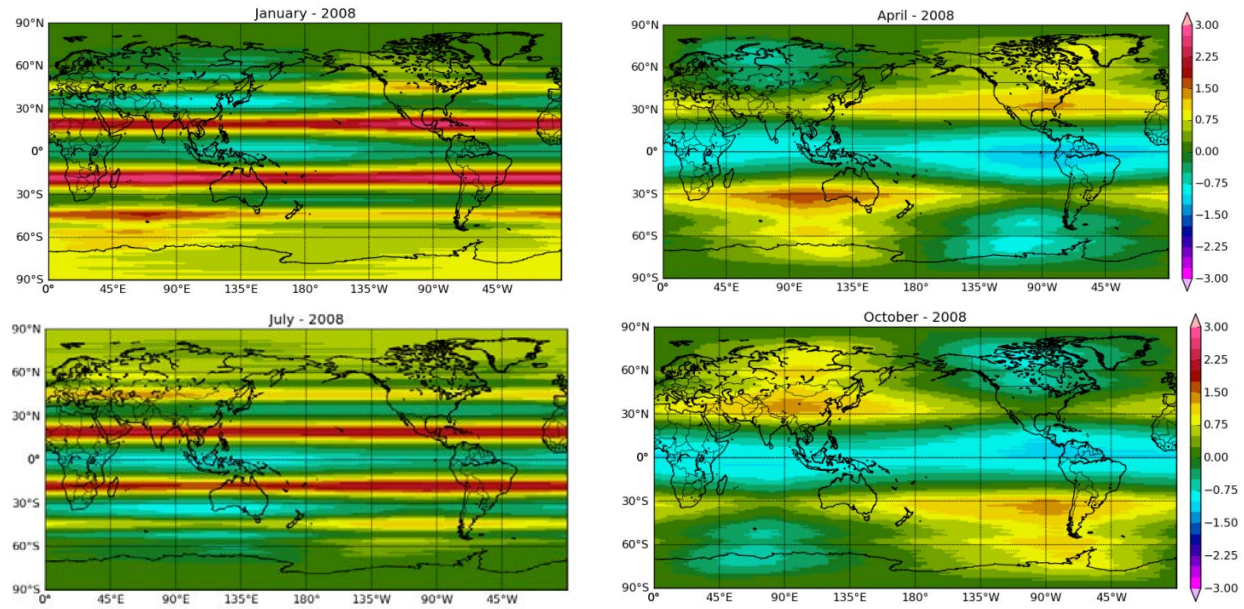

Figure 6-4. Solar irradiance difference between EBAF Ed4.0 and Ed2.8 for January, April, July and October 2008.

6.3. Trend Comparisons

While trends for EBAF Ed4.0 are generally similar to Ed2.8, there are notable differences worth mentioning. Table 6-3 provides global mean trends for EBAF Ed4.0 and Ed2.8 between March 2000 and June 2015. For all-sky SW, the EBAF Ed4.0 trend is –0.41 W m^{-2} per decade compared to –0.11 W m^{-2} per decade in Ed2.8. In contrast, trends for all-sky LW TOA flux are consistent to 0.1 W m^{-2} per decade. To understand the reason behind the SW TOA flux trend difference, we first compared results aimed at isolating Ed3 and Ed4 calibration differences (gains and time-dependent spectral response function changes) by using the same Ed2 cloud retrievals, ADMs and time interpolation methodology but with the Ed3 and Ed4 calibration coefficients. We found SW TOA flux trends to be nearly identical (within 0.07 W m^{-2} per decade). Similarly, we found negligible impact on SW TOA flux trends resulting from the use of different Ed4.0 and Ed2.8 time interpolation methodologies. This suggests the Ed4.0–Ed2.8 SW trend differences are related to cloud retrieval/ADM differences. Figure 6-5a provides time series of CERES Terra SSF1deg Ed4A minus Ed3A SW TOA flux and MODIS-derived cloud optical depth for global ocean (note that the y-axis for cloud optical depth differences has been reversed). SSF1deg Ed3A uses the same input cloud retrievals and ADMs as EBAF Ed2.8, and similarly for SSF1deg Ed4A and EBAF Ed4A. Both SW TOA flux and cloud optical depth differences show a systematic trend of opposite sign. The two fields are strongly anti-correlated (Figure 6-5b), with a correlation coefficient of –0.72.

Deseasonalized anomalies in cloud optical depth (Figure 6-6a) clearly show a much stronger decreasing trend in Ed3A than Ed4A. The reason for the cloud optical depth trend differences is due to how MODIS Terra calibration changes are accounted for in Ed3A and Ed4A. The Terra-

MODIS instrument band 1 (0.65µm) experienced two calibration anomalies over the CERES record. The first anomaly occurred on July 2, 2003 when the solar diffuser door on the Terra-MODIS malfunctioned and was left in the open position, causing the Terra-MODIS solar diffuser to degrade at a faster rate. The second anomaly occurred in early 2009, when solar diffuser degradations were observed to be 1.5% and 0.3% for Terra and Aqua-MODIS, respectively. The MODIS inputs used for EBAF Ed2.8 and SSF1deg Ed3A rely on Collection 4 through April 2006 and Collection 5 thereafter. CERES EBAF Ed4.0 uses Collection 5 for the entire record, and makes different adjustments than the earlier version to account for the Terra-MODIS calibration anomalies.

Because MODIS cloud optical depths are used to select anisotropic factors (i.e., ADM) in converting CERES radiances to radiative fluxes, the different cloud optical depth trends in Ed3A and Ed4A result in slightly different SW TOA flux trends as well (Figure 6-6b). The Ed4-Ed3 cloud optical depth trend difference corresponds to 5% per decade relative to the mean cloud optical depth, while the SW TOA flux trend difference corresponds to –0.25 W m^{-2} per decade.

For clear-sky, EBAF Ed4.0 and Ed2.8 SW TOA flux trends differ by only 0.11 W m^{-2} per decade, compared to 0.32 W m^{-2} per decade for LW. The larger difference for LW is due to a spurious discontinuity in EBAF Ed2.8 caused by a change in the source of assimilated meteorological data in January 2008 from GEOS-4.1 to GEOS-5.2.0. This change has a large impact on the nighttime cloud mask applied to MODIS pixel data for distinguishing between clear and cloud-contaminated areas. The problem is resolved in Ed4.0 as it uses GEOS-5.4.1 meteorological assimilation data throughout the CERES record. The EBAF Ed4.0 algorithm improvements result in a marked change in net CRE compared to EBAF Ed2.8: net CRE changes from -0.6 W m^{-2} per decade in EBAF Ed2.8 to -0.18 W m^{-2} per decade for EBAF Ed4.0.

Table 6-3. Global mean TOA flux/CRE trend (W m^{-2} per decade) for March 2000-June 2015. Uncertainties are at the 95% significance level and only account for interannual variations in monthly anomalies.

	All-Sky		Clear-Sky		CRE	
	Ed2.8	Ed4.0	Ed2.8	Ed4.0	Ed2.8	Ed4.0
SW	-0.11±0.16	-0.41±0.18	-0.19±0.10	-0.30±0.10	-0.07±0.15	0.11±0.18
LW	-0.02±0.14	0.07±0.15	-0.54±0.12	-0.22±0.11	-0.52±0.09	-0.30±0.10
Net	0.09±0.21	0.29±0.22	0.69±0.14	0.46±0.14	-0.60±0.15	-0.18±0.17

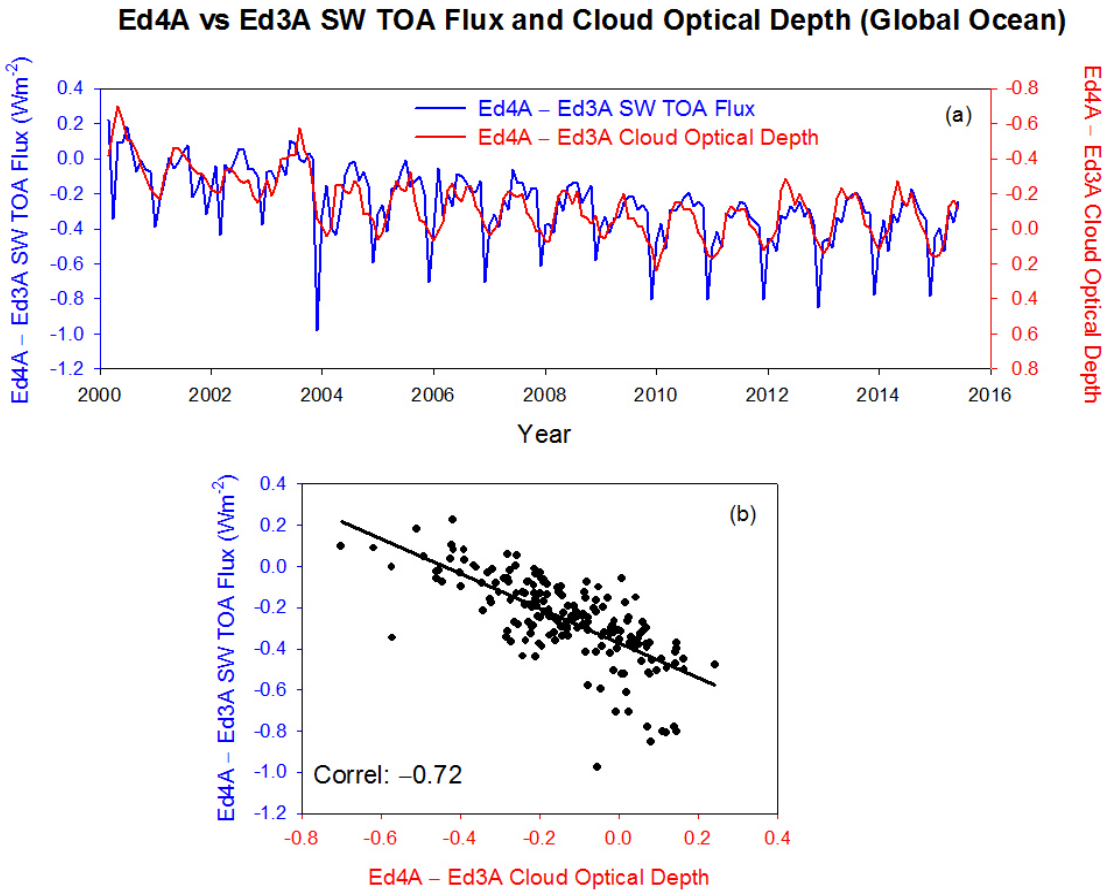

Figure 6-5. (a) Time series of Ed4A minus Ed3A SW TOA flux and cloud optical depth for global ocean and (b) scatter plot of time series shown in (a).

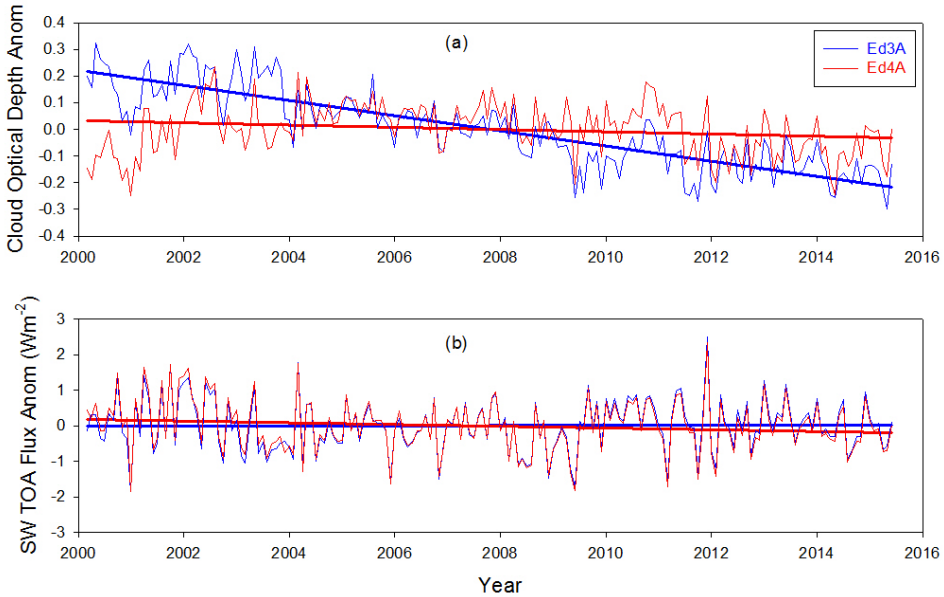

Figure 6-6. Time series of Ed3A and Ed4A anomalies in (a) cloud optical depth and (b) SW TOA flux for global ocean.

7. References

Dewitte, S., D. Crommelynck, and A. Joukoff, 2004: Total solar irradiance observations from DIARAD/VIRGO. *J. Geophys. Res.*, **109**, A02102, doi:10.1029/2002JA009694.

Dewitte, S., E. Janssen, and S. Mekaoui, 2013: Science results from the Sova-Picard total solar irradiance instrument, *AIP Conf. Proc.*, **1531**, 688-691, doi:10.1063/1.4804863.

Doelling, D. R., N. G. Loeb, D. F. Keyes, M. L. Nordeen, D. Morstad, C. Nguyen, B. A. Wielicki, D. F. Young, and M. Sun, 2013: Geostationary enhanced temporal interpolation for CERES flux products. *J. Atmos. Oceanic Technol.*, **30**, 1072-1090.

Doelling, D.R., M. Sun, L.T. Nguyen, M.L. Nordeen, C.O. Haney, D.F. Keyes, P.E. Mlynczak, 2016, Advances in Geostationary-Derived Longwave Fluxes for the CERES Synoptic (SYN1deg) Product, *J. Atmos. Oceanic Technol.* Vol. 33, March 2016: 503-521, DOI: 10.1175/JTECH-D-15-0147.1.

Hansen, J. et al. 2005: Earth's energy imbalance: confirmation and implications. *Science*, **308**, 1431–1435.

Johnson, G. C., J. M. Lyman, and N. G. Loeb. 2016. Improving estimates of Earth's energy imbalance. Nature Climate Change, 6, 639-640, doi:10.1038/nclimate3043.

Kato, S., and N. G. Loeb, 2003: Twilight irradiance reflected by the earth estimated from Clouds and the Earth's Radiant Energy System (CERES) measurements. *J. Climate*, **16**, 2646–2650.

Kato, S., and N. G. Loeb, 2005: Top-of-atmosphere shortwave broadband observed radiance and estimated irradiance over polar regions from Clouds and the Earth's Radiant Energy System (CERES) instruments on Terra. *J. Geophys. Res.*, **110**, doi:10.1029/2004JD005308.

Kato, S., N. G. Loeb, F. G. Rose, D. R. Doelling, D. A. Rutan, T. E. Caldwell, L. Yu, R. A. Weller, 2013: Surface irradiances consistent with CERES-derived top-of-atmosphere shortwave and longwave irradiances, J. Climate, 26(9), 2719-2740 . http://dx.doi.org/10.1175/JCLI-D-12-00436.1.

Kopp, G. and G. Lawrence, 2005: The Total Irradiance Monitor (TIM): Instrument design. *Sol. Phys.*, **230**, 91-109.

Kopp, G. and J. L. Lean, 2011: A new, lower value of total solar irradiance: Evidence and climate significance. *Geophys. Res. Lett.*, **38**, L01706, doi:10.1029/2010GL045777.

Loeb, N. G., K. J. Priestley, D. P. Kratz, E. B. Geier, R. N. Green, B. A. Wielicki, P. O. R. Hinton, and S. K. Nolan, 2001: Determination of unfiltered radiances from the Clouds and the Earth's Radiant Energy System (CERES) instrument. *J. Appl. Meteor.*, **40**, 822–835.

Loeb, N. G., S. Kato, and B. A. Wielicki, 2002: Defining top-of-atmosphere flux reference level for Earth Radiation Budget studies. *J. Climate*, **15**, 3301-3309.

Loeb, N. G., N. M. Smith, S. Kato, W. F. Miller, S. K. Gupta, P. Minnis, and B. A. Wielicki, 2003: Angular distribution models for top-of-atmosphere radiative flux estimation from the Clouds and the Earth's Radiant Energy System instrument on the Tropical Rainfall Measuring Mission Satellite. Part I: Methodology. *J. Appl. Meteor.*, **42**, 240–265.

Loeb, N. G., W. Sun, W. F. Miller, K. Loukachine, and R. Davies, 2006: Fusion of CERES, MISR and MODIS measurements for top-of-atmosphere radiative flux validation. *J. Geophys. Res.*, **111**, D18209, doi:10.1029/2006JD007146.

Loeb, N. G., B. A. Wielicki, W. Su, K. Loukachine, W. Sun, T. Wong, K. J. Priestley, G. Matthews, W. F. Miller, and R. Davies, 2007: Multi-instrument comparison of top-of-atmosphere reflected solar radiation. *J. Climate*, **20**, 575-591.

Loeb, N. G., B. A. Wielicki, D. R. Doelling, G. L. Smith, D. F. Keyes, S. Kato, N. Manalo-Smith, T. Wong, 2009: Toward optimal closure of the Earth's top-of-atmosphere radiation budget. *J. Climate*, **22**, 748-766, doi:10.1175/2008JCLI2637.1.

Loeb, N. G., J. M. Lyman, G. C. Johnson, R. P. Allan, D. R. Doelling, T. Wong, B. J. Soden, and G. L. Stephens, 2012: Observed changes in top-of-the-atmosphere radiation and upper-ocean heating consistent within uncertainty. *Nat. Geosci.*, **5**, doi:10.1038/NGEO1375.

Loeb, N. G., N. Manalo-Smith, W. Su, M. Shankar, and S. Thomas, 2016: CERES top-of-atmosphere earth radiation budget climate data record: accounting for in-orbit changes in instrument calibration. Remote Sensing, 8(3), 182 . http://dx.doi.org/10.3390/rs8030182.

Lyman, J. M., and G. C. Johnson, 2008: Estimating annual global upper-ocean heat content anomalies despite irregular in situ ocean sampling. *J. Climate*, **21**, 5629–5641.

Mekaoui, S., and S. Dewitte, 2008: Total Solar Irradiance measurement and modelling during cycle 23, *Sol. Phys*., **247**, 203-216.

Minnis P., S. Sun-Mack, D. F. Young, P. W. Heck, D. P. Garber, Y. Chen, D. A. Spangenberg, R. F. Arduini, Q. Z. Trepte, W. L. Smith, Jr., J. K. Ayers, S. C. Gibson, W. F. Miller, G. Hong, V. Chakrapani, Y. Takano, K.-N. Liou, Y. Xie, and P. Yang, 2011: CERES Edition-2 cloud property retrievals using TRMM VIRS and Terra and Aqua MODIS data--Part I: Algorithms. *IEEE Trans. Geosci. Remote Sens*., **49**, 4374-4400.

Purkey, S. G., and G. C. Johnson, 2010: Warming of global abyssal and deep southern ocean waters between the 1990s and 2000s: contributions to global heat and sea level rise budgets. *J. Climate*, **23**, 6336–6351.

Rhein, M. *et al.* in *Climate Change 2013: The Physical Science Basis* (eds Stocker, T. F. *et al.*) 255–315 (IPCC, Cambridge University Press, 2013).

Roemmich, D. et al., 2009: Argo: the challenge of continuing 10 years of progress. *Oceanography*, **22**, 46–55.

Sohn, B.-J., J. Schmetz, R. Stuhlmann, and J.-Y. Lee, 2006: Dry bias in satellite-derived clear-sky water vapor and its contribution to longwave cloud radiative forcing. *J. Climate*, **19**, 5570-5580.

Su, W., J. Corbett, Z. Eitzen, L. Liang, 2015a: Next-generation angular distribution models for top-of-atmosphere radiative flux calculation from CERES instruments: methodology. Atmos. Meas. Tech., 8(2), 611-632. http://dx.doi.org/10.5194/amt-8-611-2015.

Su, W., J. Corbett, Z. Eitzen, L. Liang, 2015b: Next-generation angular distribution models for top-of-atmosphere radiative flux calculation from CERES instruments: validation. Atmos. Meas. Tech., 8(8), 3297-3313. http://dx.doi.org/10.5194/amt-8-3297-2015.

Sun, W., N. G. Loeb, S. Kato, B. Lin, Y. Hu, and C. Lukashin, 2011: A study of subvisual clouds and their radiation effect with a synergy of CERES, MODIS, CALIPSO, AIRS, and AMSR-E data. *Atmos. Chem. Phys*. (submitted).

Thomas S., K. J. Priestley, N. Manalo-Smith, N. G. Loeb, P. C. Hess, M. Shankar, D. R. Walikainen, Z. P. Szewcyzk, R. S. Wilson, D. L. Cooper, 2010: Characterization of the Clouds and the Earth's Radiant Energy System (CERES) sensors on the Terra and Aqua spacecraft, *Proc. SPIE*, Earth Observing Systems XV, Vol. 7807, 780702, August 2010.

Wood, R., 2012: Stratocumulus clouds. Mon. Weath. Rev., 140, 2373-2423, DOI: 10.1175/MWR-D-11-00121.1.

Young, D. F., P. Minnis, D. R. Doelling, G. G. Gibson, and T. Wong, 1998: Temporal Interpolation Methods for the Clouds and Earth's Radiant Energy System (CERES) Experiment. *J. Appl. Meteorol*., **37**, 572-590.

8. Expected Reprocessing

There are no plans to reprocess the EBAF record until the CERES Edition 5 suite of data products are available. Any updates to the CERES EBAF product will be available for subsetting/visualization/ordering at: http://ceres.larc.nasa.gov/order_data.php.

9. Attribution

When referring to the CERES EBAF product, please include the data product and the data set version as "CERES_EBAF_Ed4.0."

The CERES Team has put forth considerable effort to remove major errors and to verify the quality and accuracy of this data. Please provide a reference to the following paper when you publish scientific results with the CERES EBAF_Ed4.0.

Loeb, N. G., B. A. Wielicki, D. R. Doelling, G. L. Smith, D. F. Keyes, S. Kato, N. Manalo-Smith, T. Wong, 2009: Toward optimal closure of the Earth's top-of-atmosphere radiation budget. *J. Climate*, **22**, 748-766, doi:10.1175/2008JCLI2637.1.

When CERES data obtained via the CERES web site are used in a publication, we request the following acknowledgment be included: "These data were obtained from the NASA Langley Research Center CERES ordering tool at http://ceres.larc.nasa.gov/."

10. Feedback and Questions

For questions or comments on the CERES Data Quality Summary, contact the User and Data Services staff at the Atmospheric Science Data Center. For questions about the CERES subsetting/visualization/ordering tool at http://ceres.larc.nasa.gov/order_data.php, please email ceres-help@lists.nasa.gov.